Nanoscale Horizons

Accepted Manuscript

ROYAL SOCIETY OF CHEMISTRY

rsc.li/nanoscale-horizons

Journal Name

ARTICLE

Exploiting the Biological Windows: Current Perspectives on Fluorescent Bioprobes Emitting above 1000 nm

Eva Hemmer,[a] Antonio Benayas,[a] François Légaré[a] and Fiorenzo Vetrone[*, a, b]

Received 00th January 20xx,
Accepted 00th January 20xx

DOI: 10.1039/x0xx00000x

www.rsc.org/

With the goal of developing more accurate, efficient, non-invasive and fast diagnostic tools, the use of near-infrared (NIR) light in the range of the second and third *biological windows* (NIR-II: 1000-1350 nm, NIR-III: 1550-1870 nm) is growing remarkably as it provides the advantage of deeper penetration depth into biological tissues, better image contrast, reduced phototoxicity and photobleaching. Consequently, NIR-based bioimaging has become a quickly emerging field and manifold new NIR-emitting bioprobes have been reported. Classes of materials suggested as potential probes for NIR-to-NIR bioimaging (using NIR light for the excitation and emission) are quite diverse. These include rare-earth based nanoparticles, Group-IV nanostructures (single walled carbon nanotubes, carbon nanoparticles and more recently Si- or Ge-based nanostructures) as well as Ag, In and Pb chalcogenide quantum dots. This review summarizes and discusses current trends, material merits, and latest developments in NIR-to-NIR bioimaging taking advantage of the region above 1000 nm (i.e. the second and third *biological windows*). Further consideration will be given to upcoming probe materials emitting in the NIR-I region (700-950 nm), thus do not possess emissions in these two windows, but have high expectations. Overall, the focus is placed on recent discussions concerning the optimal choice of excitation and emission wavelengths for deep tissue high-resolution optical bioimaging and on fluorescent bioprobes that have successfully been implemented in *in-vitro* and *in-vivo* applications.

Introduction

Optical Bioimaging

Bioimaging is a crucial tool for the investigation of biological phenomena and in the diagnosis of diseases such as cancer. Herein, optical imaging is highly complementary to other imaging methods, such as X-ray or magnetic resonance imaging, in particular due to its potential for acquisition of data at high speeds. This allows for the visualization of dynamic biological processes, events related to physiology and disease progression.[1] As the detection of diseases at the earliest stages highly increases the chance of the patient's full recovery, the need for efficient and reliable bioprobes rises. Today's clinically used fluorescent probes are most often based on organic molecules. However, they usually require excitation with high energy light (ultraviolet (UV) or blue) in order to generate the emission of visible (VIS) light. This use of UV light induces photobleaching of the organic molecules, which restricts their temporal use. Further drawbacks include the autofluorescence of the biological tissue upon UV excitation leading to reduced image contrast through background interference, and the phototoxicity of UV light towards biological matter. Moreover, UV and VIS light exhibit a limited penetration depth into and subsequently propagation out of biological samples not allowing for deep-tissue imaging. These limitations must be overcome in order to meet the demands for more efficient and reliable bioprobes for early detection and diagnosis. In this context, various approaches have been followed in research laboratories around the globe in the search for appropriate alternatives. It should be noted that in this review, the term "penetration depth" is used throughout in order to generally refer to both penetration of the excitation light into the tissue and propagation of the emitted light out of deeper tissue areas.

Near-Infrared Light as an Alternative

Exploiting the *Biological Windows*

For the development of an ideal fluorescent bioprobe, the material requirements are exhaustive. These include bright luminescence, photostability, biocompatibility, sizes allowing for clearance from the organism at the right time (overall complete clearance has to be assured in order to avoid potential long-term toxic effects, while too rapid clearance would hinder the probe's

[a] *Institut National de la Recherche Scientifique - Énergie Matériaux Télécommunications, Université du Québec, 1650 Boulevard Lionel-Boulet, Varennes (Québec), J3X 1S2 Canada.*
[b] *Centre for Self-Assembled Chemical Structures, McGill University, Montreal, (Québec), H3A 2K6 Canada*
[*] *Corresponding Author Email: vetrone@emt.inrs.ca*
† Footnotes relating to the title and/or authors should appear here.
Electronic Supplementary Information (ESI) available: [details of any supplementary information available should be included here]. See DOI: 10.1039/x0xx00000x

accumulation in the organ or tissue under observance). The materials must also possess good dispersibility in biological media, chemical stability, specificity and selectivity for targeted imaging (yet minimal non-specific biological binding), reduced autofluorescence, and optical properties allowing for deep tissue penetration of the applied excitation and emission light.[2] The use of near-infrared (NIR) instead of VIS or UV is paramount in addressing the latter demand for deep-tissue imaging, specifically when the wavelengths fall within the often referred to *biological windows*.[3-4] Within these windows, three distinctive wavelength regions have been identified: the so-called *first biological window* spans the wavelength range from 700 nm to 950 nm (NIR-I), the *second biological window* covers the region from 1000 to 1350 (NIR-II), and the *third biological window* is found from 1550 to 1870 (NIR-III),[4-6] each window providing increased transparency toward biological matter. Figure 1 highlights these *NIR windows* by presenting the wavelength dependency of the loss coefficient of human skin (Figure 1a) as well as the attenuation coefficient of blood, skin, and fatty tissue (Figure 1b).

Interaction between Light and Biological Matter

When aiming for deep-tissue optical imaging, the ability of the applied light to penetrate the tissue is the obvious key parameter. In order to be able to make an appropriate wavelength choice allowing for optimized light penetration, a basic understanding of the interactions between light and biological matter, such as scattering and absorption, is essential. *Absorption* occurs during the propagation of light in a material medium if the frequency of light is resonant with the transition frequencies of the atoms in that medium. The transmission of the medium is clearly related to the absorption, because only unabsorbed light will be transmitted. *Scattering* is the phenomenon in which the light changes direction and possibly also its frequency after interacting with the medium. The total number of photons is unchanged, but the number of photons going in the forward direction decreases because light is re-directed in other directions. Scattering therefore has the same attenuating effect as absorption.[7] In fact, much effort has been undertaken to quantify the effect of those interactions on light-propagation through tissues. For example in an early study, Anderson et al. presented a model for the optics of the human skin describing its wavelength dependent transparency (Figure 1a).[3]

Generally speaking, the stratum corneum and epidermis of human skin provide an optical barrier, where most of the incident light is blocked by absorption and also affected by optical scattering.[4] The pigment melanin has been identified as the major skin-located absorber of radiation in the wavelength region 350 to 1200 nm, especially at shorter wavelengths. However, when focusing on deep penetration depth, a careful look at biological tissues other than the skin is also deemed necessary. With regards to optical scattering, which profoundly affects the penetration of light through tissues,[8] the *reduced scattering coefficient* has been introduced as the quantitative variable that accounts for both wavelength and angular dependence of scattering. In human subcutaneous adipose tissue, it has been shown that the *reduced scattering coefficient* decreases smoothly with increasing wavelength in the spectral range from 400 to 1500 nm, while it increases with oscillations (peaks corresponding to the absorption bands) in the spectral range 1500 to 2000 nm.[9] Taking into account the possible penetration depth reducing (and wavelength-dependent) effect of optical scattering, the use of longer wavelengths (further into NIR range) for both the excitation and emission wavelength becomes favourable for *in-vivo* imaging. The need for deeper understanding of the specific optical properties of biological tissues for proper design of devices, interpreting diagnostic measurements or planning therapeutic protocols was also stated by Jacques.[10] The recent review paper provides an overview of the scattering and absorption behaviour of several groups of tissues. This includes scattering coefficients of skin, brain, breast, bone, other soft tissues, other fibrous tissues and fatty tissues, as well as the absorption coefficients for blood, water, melanin, fat, and yellow pigments. Moreover, it was shown that optical scattering not only affects the penetration depth, but also reduces the optical contrast, which obviously is highly disadvantageous for well-resolved sub-tissue fluorescence images. Regarding autofluorescence in the NIR region above 1000 nm, a very recent paper from Diao at al. establishes the existence of preferred spectral ranges, where autofluorescence from endogenous sources is minimal. Specifically under 808 nm excitation, the 1500 to 1700 nm region can afford nearly zero tissue autofluorescence, thus allowing for much better optical contrast from the potential exogenous bioprobes emitting fluorescent signals that match those specific ranges.[11]

As a consequence of further development, the field of *in-vivo* NIR-emitting bioprobes is seeing a more pronounced shift towards the NIR-II and NIR-III regions as it is generally assumed that the *reduced scattering coefficient* decreases with an increase in the wavelength. Yet, overall, it must be kept in mind that light-tissue interactions may also be dependent on patient-specific tissue characteristics and biological circumstances, making it non-trivial to predict the optical tissue properties.

Recent Trends in the Development of NIR-to-NIR Bioprobes

Seeing the drawbacks of commonly used bioprobes operating in the UV-VIS region, current research trends in the field of optical bioimaging are shifting from the UV-VIS region to the NIR *biological windows*. Moreover, with the commercialization of affordable InGaAs cameras that possess adequate sensitivity and resolution as well as high enough quantum efficiency in the wavelength region above 1000 nm,[4] *in-vivo* imaging utilizing NIR-II and NIR-III emitters has become more accessible. This clearly contributes to the increasing interest in the development of

novel NIR-to-NIR bioprobes, particularly those emitting light with wavelengths longer than 1000 nm. Herein, the materials of interest span from organic molecular compounds to organic / inorganic nanostructures and quantum dots (QDs).

When it comes to fluorescent imaging probes that made the leap from research to clinical use, organic dyes are the most commonly applied. Among them, indocyanine green is an example of an FDA (U.S. Food and Drug Administration) approved NIR-I-to-NIR-I dye absorbing at a wavelength of about 800 nm and showing maximum emission at 830 nm (in blood).[12-13] To date, most reported organic NIR dyes absorb and emit in the NIR-I region.[14] However, motivated by the various advantages of the NIR-II and NIR-III regions, progress has been made on the development of novel organic dyes for NIR-to-NIR bioimaging.[15] As a result of recent efforts, promising candidates have been reported with significantly improved water-solubility, quantum yield (QY), stability, detection sensitivity and emission wavelengths longer than 1000 nm for *in-vivo* imaging, thus targeting the NIR-II region as described in more detail in a later section. As an alternative class of bioprobes, heavy-metal based semiconductor QDs such as CdTe or CdSe show bright size-tuneable luminescence with high QY; mostly within the NIR-I region (700 to 950 nm). Excellent research and review papers have already been published discussing their applications to bioimaging.[16-22] However, the emission wavelength of these conventional heavy-metal based semiconductor QDs is limited to the range shorter than 1000 nm. In the context of the search for NIR-II and NIR-III-emitting semiconductor QDs, promising alternative chalcogenide QDs have been discovered [20-21, 23-24] that will be described in more detail in the later sections of this review. Thus, aside from NIR-II and NIR-III emitters, special consideration will be given to up and coming fluorescent nanomaterials that, as of yet, do not possess emissions in the NIR-II and NIR-III windows, but have high expectations including carbon-dots, germanium or silicon nanoparticles, lead or indium chalcogenide QDs as well as organic probes.

Evaluating research efforts and achievements on probes emitting in the NIR-II and NIR-III *biological windows* upon NIR excitation, we identified three major groups of materials that are, to date, attracting particular attention within the NIR-to-NIR bioimaging field: (1) **rare-earth (RE^{3+}) based nanoparticles**, (2) **Group-IV nanostructures** based on silicon, germanium and carbon, as well as (3) **alternative chalcogenide QDs** based on silver, indium and lead. Among these, RE^{3+}-based nanoparticles, single-walled carbon nanotubes (SWCNTs) (a representative of Group-IV probes), and silver chalcogenide QDs (a representative of alternative chalcogenide QDs) are currently at the forefront of the race, both from the point of view of probe development and *in-vitro*/*in-vivo* testing. Excellent comprehensive review papers have been published generally describing the wide field of fluorescent nanostructures for biomedical applications for instance by Amiot et al.[25] (2008), Hahn et al.[26] (2011), Cassette et al.[27] (2013), Yao et al.[28] (2014), Li et al.[29] (2014), Pichaandi et al.[30] (2014), Peng et al.[31] (2015), Wolfbeis[32] (2015), or Prodi et al.[6] (2015). This review will highlight the above mentioned cutting-edge candidates focusing on those whose *in-vitro* and/or *in-vivo* evaluation has been reported.

Regarding the physical mechanisms for the generation of NIR light, we would like to refer at this point to research and review papers that previously have been published for RE^{3+}-based systems (dielectric host doped with optically active ions),[33-36] semiconductor QDs, specifically II-VI and II-IV QDs (inter-band transitions / excitonic recombinations),[37] semiconductor Group-IV nanostructures (vacancies, trap-states and surface-defects as fluorescence sources),[38-41] SWCNTs (radiative decay of electron-hole bound states, i.e. excitons as local zero-dimension-like states embedded in one-dimensional carbon nanotubes),[42-44] and organic dyes (electron transitions between molecular electronic states).[25] At this point, we now aim to turn the reader's attention to a selection of the most promising NIR-to-NIR bioprobes reported over recent years.

Rare-Earth Based NIR-to-NIR Bioimaging

Rare-earth (RE^{3+}) (or lanthanide, Ln^{3+}) containing compounds are well known for their outstanding optical properties, which can be attributed to the electronic structure of the 4*f* elements, namely the shielding effect of the outer $5s^2$ and $5p^6$ shells surrounding the 4*f* electrons in the RE^{3+} ions.[45] As a consequence, there is only little influence of the environment on the emission behaviour of RE^{3+}; sharp emission as well as excitation spectra, and large Stokes shifts are characteristic for these types of materials, which makes them highly interesting for imaging applications.

NIR-II and NIR-III Emission from RE^{3+}-doped Nanoparticles

In the race for the development of NIR-to-NIR bioprobes, upconverting nanoparticles (UCNPs) co-doped with thulium (Tm^{3+}) and ytterbium (Yb^{3+}) ions have raised interest due to their NIR-to-NIR upconversion resulting in the NIR-I emission of 800 nm light following excitation with 980 nm and matching with the *first biological window*.[46-49] Yet, in order to take advantage of the reduced scattering and therefore expected deeper penetration depth of light with wavelengths longer than 1000 nm, on-going research is putting effort in the development of RE^{3+}-based nanoparticles that emit light in the NIR-II or NIR-III *biological windows*. In this context, Ho^{3+}- or Er^{3+}-doped nanoparticles have been reported as excellent candidates given that they possess emissions at ~1200 nm (Ho^{3+}, NIR-II) and 1550 nm (Er^{3+}, NIR-III), respectively. Here, for the generation of NIR-II or NIR-III light, one higher energy photon (NIR-I) is converted into one lower energy photon (NIR-II or NIR-III). This mechanism is in contrast to the above mentioned upconversion process, where at least two low energy photons (NIR-I, 980 nm) are converted into one higher energy photon (NIR-I, 800 nm). Besides Er^{3+} or Ho^{3+}, most

often Yb^{3+} ions are applied as a co-dopant in RE^{3+}-based nanoparticles; mainly due to the excellent absorption cross-section of Yb^{3+} with 980 nm excitation light. In fact, the very good absorption of 980 nm light by Yb^{3+} (the sensitizer ion), followed by the energy transfer to RE^{3+} ions such as Er^{3+} and Ho^{3+} (the activator ion), and the eventual emission of NIR light (NIR-II, NIR-III) makes 980 nm a very popular excitation wavelength even though it does not, strictly speaking, match with one of the *biological windows*. While much work has been carried out focusing on the spectroscopic characterization of NIR-II and NIR-III-emitting RE^{3+}-doped nanoparticles, their implementation into biological environments such as cells or small animals for *in-vitro* and *in-vivo* bioimaging is still relatively scarce, though highly promising.

The first non-specific (without targeting a specific organ, cell or tissue type such as tumorous tissue) *in-vivo* imaging of a small animal by use of NIR-I excitation generating NIR-III emission was reported in 2011 by the group of K. Soga.[50] Upon injection of Er^{3+}/Yb^{3+} co-doped Y_2O_3 nanoparticles *via* the tail vein of mice, *in-vivo* images of the whole mouse body were recorded detecting the 1550 nm emission from Er^{3+} ions following 980 nm excitation. Clear NIR-III luminescence was observed from the liver of the mouse without any dissection, which proves the suitability of RE^{3+}-based nanoparticles for *in-vivo* bioimaging above 1000 nm. Further investigation of the biodistribution in the organs after dissection of the mice showed highest luminescence from the clearance organs (liver and spleen) as well as the lung. Aside from their optical features, chemical surface modification of the nanoparticles was demonstrated to be crucial in the application of the bioprobes since agglomeration under biological conditions causes severe problems and can be fatal to the animal due to clogging of the blood vessels. Yet, through appropriate surface modification of the Er^{3+}/Yb^{3+}:Y_2O_3 nanoparticles with, for example, a poly(ethylene glycol) (PEG) based block co-polymer, long-term dispersion stability (up to seven days) was achieved. The excellent dispersion stability was assigned to only minimal non-specific interactions of PEG-modified nanoparticles with serum proteins. Further efforts have been undertaken by the same group resulting in not only Er^{3+}-based NIR-III emitters, but also Ho^{3+}-based NIR-II emitters that have successfully been applied *in-vivo*. Two recently published review papers provide deeper insight into the *in-vitro* cytotoxicity and *in-vivo* biodistribution of these RE^{3+}-doped Y_2O_3 and Gd_2O_3 nanostructures as a function of their morphology, size and surface chemistry.[51-52] Generally speaking, RE^{3+} ions are not considered as highly toxic. Yet, they may interact with proteins and biological molecules when applied *in-vitro* or *in-vivo*, which may disturb the electron/ion cell membrane transport activity eventually inducing cell damage. In the NIR bioprobes discussed here, based on e.g., $NaGdF_4$ or $NaYF_4$, the RE^{3+} ions are embedded in a dielectric host matrix. Consequently, the surface reactivity of these nanoparticles should be limited only to RE^{3+} ions exposed on their surface.[53] Still, RE^{3+} ions may leak from the surface as observed in case of Y_2O_3 or Gd_2O_3. Approaches applying for instance PEG-based surface modification have been shown as suitable to prevent this release of RE^{3+} ions from the host material.[54-55] Further studies addressed the potential long-term (up to 3 months) *in-vivo* toxicity of RE^{3+}-doped PEG- or poly(acrylic acid) (PAA)-modified $NaYF_4$ in mouse studies providing highly promising results.[56-57] Clearly, more comprehensive studies are required for further toxicity assessment of RE^{3+}-based bioprobes in order to draw a full image of their potential *in-vivo* toxicity. However, the negligible or low toxicity of RE^{3+}-based probes reported to date is highly encouraging and has led to various applications in biomedicine, including theranostic approaches beyond NIR-NIR bioimaging.[58-61] On-going developments of NIR-II and NIR-III suitable RE^{3+}-based bioprobes also triggered the technological evolvement of prototypes for portable imaging systems. For instance, the group of K. Soga developed NIS-Opt (Shimadzu, Kyoto, Japan), an NIR-to-NIR bioimaging system that is equipped with laser diode excitation at 980 nm and InGaAs CCD allowing for the detection in the NIR-II and NIR-III regions.[51, 62-63]

Another important aspect that must generally be considered when aiming to implement fluorescent nanoparticles in imaging applications is the need for minimal uncontrolled circulation in the blood system and eventual trapping of the nanoparticles in the clearance organs such as liver and spleen. In contrast, specific imaging (targeted imaging of specific cells or tissues) has to be enabled. In this context, the suitability of streptavidin conjugated Er^{3+}/Yb^{3+}:Y_2O_3 nanoparticles for NIR-III-based targeting of cancer cells and human colon cancer tissue has been shown. The streptavidin conjugated to the surface specifically binds to the biotinylated antibodies expressed on cancer cells and consequently allows for specific imaging.[64] Targeting deep-tissue imaging, the same study further shows high contrast images that could be recorded through a 1 cm thick sample of porcine meat, which is physiologically and optically similar to human tissue and therefore considered as a suitable pre-human validation model.

Addressing the need for specific imaging, Naczynski et al. encapsulated RE^{3+}:$NaYF_4$ nanoparticles in albumin prior to application of the nanocomposite for *in-vivo* NIR-I-to-NIR-II,III bioimaging.[65] The resultant RE^{3+}-albumin-nanocarriers showed increased bioactivity when compared to RE^{3+}-based nanoparticles only. As a consequence, the nanocarriers underwent strong accumulation in tumorous tissues and were proven as efficiently targeting NIR-to-NIR probes in melanoma bearing mice. The visualization of organs and tumours were obtained at video-rate while micrometre resolution and millimetre depths were achieved. Moreover, the authors provide a comparison of the different scattering behaviour of emitted NIR-I (808 nm) and NIR-III (1525 nm) light. Very interesting with regard to the envisaged high-resolution deep-tissue bioimaging, improved resolution quality and deeper penetration depth were

observed for the emission signal in the longer wavelength range (NIR-III) (Figure 2). These findings clearly stress the need for shifting the emission wavelength range of NIR-to-NIR bioprobes for optical deep-tissue imaging to the NIR-II and NIR-III region.

RE^{3+}-based NIR-to-NIR Probes: Choosing the Right NIR Excitation Wavelength

As stated earlier, Yb^{3+} is the most commonly applied co-dopant and sensitizer in RE^{3+}-doped nanoparticles. However, during the last few years, Nd^{3+} is gaining growing recognition as a sensitizer due to its large absorption cross-section and QY. As a consequence, Nd^{3+}-doped NIR-I-to-NIR-II and NIR-I-to-NIR-III nanoparticles have aroused interest among researchers working in the field of NIR-emitting RE^{3+}-based bioprobes. The replacement of the Yb^{3+} sensitizer ion by Nd^{3+} allows for excitation with light in the range of 800 nm rather than 980 nm. In fact, the choice of the excitation wavelength is vital when aiming for an enhancement of the tissue penetration and minimization of potential photo-damage to the biological tissue. It has been shown that the water absorption of 800 nm light is significantly lower than that of 980 nm. Thus, the effects of overheating on tissues could be reduced. These observations are assigned to a 60 % weaker energy attenuation of the 800 nm light when compared to 980 nm after passing through water.[66] This makes nanoparticles doped with Nd^{3+} very promising candidates for deep-tissue imaging. For instance, NIR-to-NIR bioimaging using a core/shell structure Nd^{3+}:$NaGdF_4$/$NaGdF_4$ was initially demonstrated by the group of P. N. Prasad.[67] NIR-II emission at 1050 nm from the $^4F_{3/2}$ state to the $^4I_{11/2}$ state of Nd^{3+} ions was obtained under NIR-I (740 nm) excitation. Wang et al.[66] developed a more complex core / multishell nanoparticle architecture in $NaGdF_4$ /Er^{3+}:$Na(Gd,Yb)F_4$ / Yb^{3+}:$NaYF_4$ / Yb^{3+}:$NaNdF_4$ that was coated with amphiphilic phospholipids for bioimaging applications. The observed bright Er^{3+}-based NIR-III emission (1550 nm) is noteworthy seeing that no direct excitation of Yb^{3+} with a 980 nm laser was performed, but an indirect excitation with 800 nm (Scheme 1). Moreover, NIR-II (1060 nm from Nd^{3+} in Nd^{3+}:$NaGdF_4$/$NaGdF_4$) and NIR-III (1525 nm from Er^{3+} in the core / multishell system) signals were compared after passing through pork muscle tissues of various thicknesses. Prior to the application of the tissues, the authors matched the emission power of the probes and the output power of the NIR excitation source to have identical spectral intensities allowing for such comparison. It was found that the penetration depth was significantly higher for the NIR-III emission originating from Er^{3+} than the NIR-II emission from Nd^{3+} after NIR-I (800 nm) excitation. Additional *in-vivo* imaging on nude mice with various probe concentrations in the stomach showed brighter NIR-III signals at lower concentration (thus a lower detection threshold) when compared to the NIR-II emission. Again, this study clearly highlights the importance of the proper wavelength choice, not only in terms of emission (optimization in the NIR-III region), but also in terms of excitation (reduced water absorption and photo-damage at ~ 800 nm).

Other types of Nd^{3+}-doped fluoride nanoparticles are also of interest.[68-70] For instance, a recent study on Nd^{3+}-doped SrF_2 from the group of D. Jaque revealed an interesting aspect addressing the problem of background fluorescence.[69] Here, it must be kept in mind that it is essential to avoid any background fluorescence when seeking high contrast bioimaging. It has been demonstrated that mouse food exhibited a strong NIR-I and NIR-II autofluorescence up to about 1100 nm when excited with 808 nm (Figure 3). The use of the emission at 1300 nm originating from the Nd^{3+} $^4F_{3/2} \rightarrow {}^4I_{13/2}$ transition permitted to overcome this drawback and resulted in deep tissue, autofluorescence free and high-resolution *in-vivo* imaging in the NIR-II window. Additionally, the authors demonstrated that the applied Nd^{3+}:SrF_2 nanoparticles did not reveal any significant toxic effect upon intravenous injection of a dose required for high-resolution *in-vivo* imaging.

To draw some conclusion from the above summarized efforts and achievements on RE^{3+}-based NIR-emitters for *in-vivo* imaging, three major observations concerning wavelength and material choice can be highlighted. First, an emission wavelength longer than 1000 nm is clearly advantageous over shorter wavelengths for high resolution imaging and deeper sub-tissue penetration. Second, regarding the appropriate wavelength choice for the excitation of the probes, the use of 800 nm (absorbed by Nd^{3+}) instead of 980 nm (absorbed by Yb^{3+}) has been proven to be highly beneficial. Third, fluoride-based nanoparticles are among the most intensively studied RE^{3+}-based bioprobes for pre-clinical *in-vitro*/*in-vivo* applications to date. Yet, the search for novel RE^{3+}-based nanomaterials suitable for efficient NIR-II and NIR-III emission is on-going, which raises expectations about their future *in-vitro* and *in-vivo* applications in high-resolution deep-tissue bioimaging. Finally providing some further perspective, progress is seen with regard to the development of RE^{3+}-based nanostructures that are not only suitable for NIR-to-NIR bioimaging, but that can also act as nanocarriers for multimodal functionalities. One example is the exploitation of the capability of Nd^{3+} to act as a photothermal agent and optical thermometer;[59, 71-72] more precisely its ability to produce substantial heating and detect it optically, which opens the avenue towards novel controlled hyperthermia-based therapy approaches.[73]

Carbon Dots and Carbon-based Nanoparticles for NIR Imaging

Among the Group-IV nanostructures, carbon nanoparticles (also known as carbon dots (C-dots); in the following referred to as carbon nanoparticles (CNPs)) have been reported to be promising novel bioprobes due to their tuneable emission-color and non-blinking of their luminescence. Moreover, CNPs are

comprised of non-toxic elements, and to date available *in-vitro* data reveal no or low cytotoxicity.[74] Still, the development of NIR-to-NIR bioprobes that match with the *biological windows* has just begun. For instance, CNPs have successfully been applied in biological imaging, whereas NIR light has either been used for the generation of light in the VIS range (multiphoton excitation), or NIR emission could be obtained under excitation with UV light.[74-76] In 2013, Yan et al. reported the synthesis and characterization of CNPs with an average size of 100 nm that possessed strong emission at 705 and 685 nm following excitation with 632.6 nm light, which approaches the NIR-I region.[77] Wu et al. prepared CNPs of less than 20 nm in diameter in a honey-based synthesis.[78] In this work, the special interest is the enhanced NIR-I emission after NIR-I excitation that could be achieved by grafting the CNP surface with a hyper-branched polymer when compared to linear PEG chains. This improvement of the optical properties was assigned to the increasing surface area available for light passivation upon more extensively branched grafting. Moreover, negligible loss of cell viability was observed upon incubation of 2F2B endothelial cells with the PEG grafted CNPs making them promising for *in-vivo* applications. In fact, *in-vivo* experiments demonstrated exceptionally rapid agglomeration and subsequent signal enhancement in lymph nodes in a mouse model. Thus, clinical potential can focus, for example, on applications during a sentinel lymph node biopsy.

Single Wall Carbon Nanotubes

While CNPs for NIR-to-NIR bioimaging are still at a very early research stage, single wall carbon nanotubes (SWCNTs) currently constitute one of the three most accomplished groups of NIR-II and NIR-III emitting *in-vivo* nanoprobes. During the last decade, SWCNTs found manifold potential applications due to their size, shape, unique structure and extraordinary physical properties in the fields of biological sensing of biomolecular species including DNA, proteins and small molecules, imaging, hyperthermia, or as drug-vehicles.[44, 79-83] This is primarily because SWCNTs show strong optical absorption and emission in the NIR *biological window*, which makes them highly attractive for deep-tissue imaging. An overview of synthetic approaches for NIR fluorescent SWNTs and their application in sensing and optical bioimaging from 2002 to 2011 was published by Huang et al. and provides a good insight into the earlier works on SWCNTs.[84]

Among the earliest developments in the field of SWCNTs for NIR bioimaging, Cherukuri et al. reported SWCNT-based fluorescence imaging of single macrophage-like cells. This early application of SWCNTs revealed high contrast imaging from the intracellular SWCNTs despite their reported low QY.[85] Herein, the authors highlight the advantage of (1) using emission wavelengths above 1125 nm instead of commonly applied shorter wavelengths in the 750 to 1100 nm region, and (2) of the very large shifts between VIS excitation (660 nm) and NIR-II,III emission (1125 to 1600 nm) wavelengths. Seeking the use of not only emission, but also excitation in the NIR region, significant work by Welsher et al. reports selective probing and imaging of cells with SWCNTs as NIR fluorescent probes.[86] In their approach, the authors functionalized SWCNTs with PEG and additionally conjugated the antibody Rituxan to the PEGylated surface. Rituxan specifically binds to the CD20 cell surface receptor on Raji cells (B-cell lymphoma). Following binding of the Rituxan-modified SWCNTs to the CD20 receptor, Raji cells were visualized by detecting the NIR fluorescence from 900 to 1600 nm under NIR-I (785 nm) excitation. Further, Choi et al. demonstrated *in-vitro* that a combination of NIR-I emitting SWCNTs with iron oxide (Fe_2O_3) nanoparticles provides a potential multimodal opto-magnetic bioprobe.[87] Consequently, after first successful applications of SWCNTs in NIR-II and NIR-III cellular imaging, *in-vivo* imaging of live animals peaked the interest of researchers in the field. In another seminal work, the group of H. Dai achieved high-frame-rate video NIR-II imaging of mice by use of DSPE-mPEG (1,2-distearoyl-sn-glycero-3-phosphoethanolamine-N-[methoxy polyethylene glycol)5000]) modified SWCNTs.[88] SWCNTs were observed in real time in the inner organs including lungs and kidneys, followed by the spleen and liver. The time-resolved study in combination with principal component analysis (PCA, a statistical processing method for compressing high-dimensional data into a lower-dimensional form) resulted in dynamic contrast-enhanced imaging providing high-resolution images of the mouse anatomy (Figure 4). The authors also critically addressed the relatively low QY of SWCNTs emphasizing the need for controlled surface modification for QY enhancement.[89] As a further example showing the importance of surface chemistry control, Robinson et al. prepared SWCNTs that are characterized by a long circulation in the blood with a half-life of about 30 h.[90] Such an extreme half-life could be achieved through surface modification with C_{18}-PMH-mPEG (poly(maleic anhydride-alt-1-octadecene)-poly(ethylene glycol) methyl ether). Moreover, it was also demonstrated that these NIR-II emitting modified SWCNTs underwent ultrahigh tumour uptake (~ 30 % of the injected dose) and accumulated in 4T1 murine breast tumors in Balb/c mice as observed by detection of the NIR-II emission. The same group performed NIR-II *in-vivo* vascular imaging[91] and most recently presented through-skull NIR-II fluorescence imaging of the brain[92]. As shown in Figure 5, non-invasive, high-resolution fluorescence imaging of mouse brain vasculature without craniotomy became possible by use of SWCNTs that emit in the NIR-II window.

These findings clearly demonstrate that SWCNTs are one of the most-developed NIR-to-NIR probe systems in terms of high-resolution, penetration depth and specific imaging. Proof-of-concepts demonstrated the potential of SWCNTs for biomedical imaging applications and future progress is expected to lead to powerful novel NIR-to-NIR bioprobes.

A critical issue that must be addressed is the toxicity assessment of SWCNTs. Given their needle-like rigid character

(that was found to induce severe health problems in case of polymer-based materials with similar morphology[93]), comparison with pathogenic asbestos may be drawn.[94] Major factors influencing cytotoxicity, inflammatogenicity, carcinogenicity, and genotoxicity were attributed by several experts in the field to the physical properties (diameter, length, aspect ratio) as well as surface modification of the SWCNTs.[95-96] Specifically, the length-dependence of the toxicity was investigated by Becker et al. resulting in an estimated critical length of 189 ± 17 nm. Below this value, the toxicity towards IMR90 human fibroblast cells was found to increase.[97] Also, it is important to mention that the findings about potential harm obtained so far have not yet resulted in an overall consensus in the field. While S. Toyokuni summarizes in his review from 2013, that no carcinogenicity has been reported for SWCNTs,[96] a study from the same year by Castranova et al. reports acute pulmonary inflammation and injury, dose-dependent rapid and persistent formation of granulomatous lesions or rapid and progressive alveolar interstitial fibrosis at deposition sites. Moreover, oxidant stress was observed that eventually triggered cardiovascular effects.[98] The increased risk of cardiopulmonary diseases after pulmonary exposure was also more recently reported by Moller et al.[99] Essential with regard to bioimaging applications, where SWCNTs may be intravenously delivered to the site of interest, is the assessment of the hemotoxicity of SWCNTs; yet, a limited amount of data has been collected over the last few years, which hampers its evaluation.[100] Thus, in order to guarantee the safety of SWCNT producers and users as well as to avoid unforeseen drawbacks on the way towards novel NIR-to-NIR bioprobes, their toxicity concerns will have to be addressed carefully in future studies by the materials, biology, toxicology and medical community.

Forthcoming Perspectives Among New Group-IV Nanoprobes

Towards Silicon-Based based NIR Probes

Another Group-IV elements recently attracting attention for NIR imaging is silicon (Si). To date, no blinking or photobleaching has been reported. Furthermore, Si, SiO_2 or SiC QDs, nanocrystals and nanoparticles become highly interesting for biomedical imaging taking into account the promising results concerning their biocompatibility [39, 101] or even biodegradability [102]. Several studies have proven that water-dispersible Si-based nanocrystals with stable emission in the NIR-I region can be synthesised, whereas a significant further red-shift into the NIR-I region is observed upon growth of the nanocrystals. Moreover, the suitability of Si-based systems for *in-vitro* and *in-vivo* imaging has been demonstrated.[103-104] However, a major challenge remains with respect to NIR-to-NIR deep-tissue imaging. In fact, all NIR-I emitters reported to date require excitation with UV-VIS light. A few groups addressed this issue by employing multiphoton excitation with femtosecond lasers in the NIR-I region. Falconieri et al. reported the two-photon-excited (excitation at 900 nm) luminescence at 750 nm from chemically oxidized pyrolytic Si nanocrystals.[105] In a similar approach, Henderson et al. demonstrated the NIR-I emission at 750 nm under two-photon NIR-I excitation (810 nm) from 4.4 nm Si nanocrystals.[106] Aside from two-photon absorption, a three-photon absorption process was reported by He et al. resulting in 650 nm VIS emission under 1335 nm NIR-II excitation of Si QDs.[107] Overall, the group of Si-based structures provides promising candidates for bioimaging applications, particularly when future efforts will allow for further tuning of the optical properties into the *biological window*.

Germanium-Based NIR-NIR Probes

In the series of Group-IV nanostructures, germanium (Ge) nanocrystals (NCs) have so far attracted only little attention. However, they have excellent potential as NIR-to-NIR bioprobes.[40] This assumption is based on reports about Ge NCs showing suitable optical properties for NIR-to-NIR bioimaging. For instance, NIR-II emission in the range 900-1400 nm under NIR-I (808 nm) excitation of colloidal Ge NCs was first reported by Lee et al.[108] Ruddy et al. reported the synthesis of size- and bandgap-controlled Ge NCs resulting in an absorption range of 780-1800 nm, whereas emission was observed in the range 860-1230 nm.[109] Interestingly, these wavelength ranges are in perfect overlap with the NIR-I, NIR-II and NIR-III windows. Moreover, they have been shown to be biocompatible when a suitable surface coating is applied, resulting in materials that are highly attractive for biomedical applications.[101] Still, potential cytotoxicity cannot be entirely ruled out yet as demonstrated in the work of Ma et al.[110] Dissimilar toxic behaviour was reported for Ge NCs depending on their preparation method. While Ge NCs obtained by a vapour-condensation process (vpGeNP, no size information provided) did not reveal any cytotoxic effect, water dispersible Ge NCs (wsGeNP, size: 4.2 ± 1.2 nm) synthesized by a reverse micelle approach showed high toxicity to cells. Here, the different physical properties of the two systems, mainly their stability towards dissolution and aggregation in water undoubtedly play a major role. Consequently, prior to future applications of Ge NCs as NIR-to-NIR bioprobes, a careful and profound risk assessment is required. Also, while live cell imaging with Ge NCs emitting light in the NIR-I range upon excitation with VIS light was very recently shown by Karatutlu et al.[111], to date, there are no reports describing *in-vitro* or *in-vivo* NIR-to-NIR bioimaging with these nanomaterials. A reason for this might be their sensitivity towards oxidation,[27] which will have to be solved before Ge-based NCs can be used as NIR-to-NIR probes for biomedical applications.

Silver Chalcogenide QDs for Imaging in the *Second Biological Window*

Particularly during the last three years, fundamental progress has been achieved on silver (Ag) chalcogenide QDs as NIR-II-emitters. A recently published review paper focusing solely on Ag chalcogenides has discussed the synthesis approaches as well as their *in-vitro* and *in-vivo* NIR imaging applications.[112] We will highlight here some of the most recent achievements in the field of Ag chalcogenide QDs, mainly Ag_2S, which has been successfully applied in several remarkable studies concerning the assessment of their NIR emission within the *biological window*, the evaluation of their cytotoxicity, and their implementation in *in-vitro* and *in-vivo* systems with regards to potential clinically relevant applications.

Ag_2S for Cellular Imaging

Fortunately, several studies indicate a good biocompatibility of Ag_2S QDs that may be advantageous for application in a biological mileu.[113-116] Aside from their biocompatibility, the representative examples of the latest generation of Ag_2S QDs present tuneable emission in the NIR-I and NIR-II regions from 687 to 1294 nm [113-116], high photoluminescence stability, relatively high QY when compared to first reported Ag_2S QDs (e.g. 2.3 % [116], 2.5 % [113], 14.2 - 16.4 % [115]), and small diameters (3.7 nm [113], 1.6 - 6.8 nm [114], 2.6 - 3.7 nm [115], 3.5 nm [116]). These properties are highly favourable for the eventual application of Ag_2S QDs in cellular and living animal imaging. In 2012, the first cellular imaging using NIR-II emission (under 658 nm illumination) was described by Zhang et al.[117] The reported hydrophobic 5.4 nm sized Ag_2S QDs were rendered hydrophilic by surface modification with dihydrolipoic acid (DHLA) exhibiting a carboxylic acid group for further biomolecular conjugation. Subsequent encapsulation with PEG allowed for a significant increase in photoluminescence QY through protection of the Ag_2S surface from the environment (15.5 % for PEG-DHLA-Ag_2S *versus* 5.8 % for DHLA-Ag_2S). Additionally, the authors demonstrated the suitability of the QDs for specific targeting to two membrane receptors that are expressed at different levels on human breast cancer cells and human glioblastoma cells. A further study reports NIR-II-based imaging of L929 cells incubated with Ag_2S QDs conjugated chitosan nanospheres that emit at 1100 nm (NIR-II) upon 808 nm (NIR-I) excitation.[118] These nanospheres could be further conjugated with S-nitrosothiol, a donor for nitric oxide (NO) that is known as a therapeutic agent. Light triggered NO release could be achieved by illumination with light in the UV and VIS regions, while the excitation with NIR-I light did not trigger the NO release. This provides an excellent example for the rational design of multifunctional Ag_2S QDs as NIR fluorescent probe and therapeutic agent.

Ag_2S for *In-Vivo* NIR-to-NIR Bioimaging

Glutathione (GSH) is known to be an abundant natural tripeptide that is found within almost all cells with much higher than normal concentrations in cancer cells. This allows for the intracellular synthesis of GSH-stabilized Ag_2S QDs in cultured cancer cells as demonstrated by Tan et al.[119] Optical properties similar to those of QDs synthesized by a conventional chemical approach (not intracellular) were found, namely absorption at 744 nm and emission at 945 nm qualifying these QDs as NIR-I probes. Subsequent NIR-I imaging has been achieved *in-vitro* upon incubation with HepG2 cells as well as *in-vivo* upon subcutaneous injection of the intracellularly synthesized Ag_2S QDs in mice. Bearing in mind the advantages of NIR-II-emitting bioprobes over those emitting in the NIR-I window, the remarkable work by Hong et al. reported the synthesis of PEGylated Ag_2S QDs showing bright emission (QY ~ 15.5 %) of NIR-II light with a maximum at 1200 nm after NIR-I excitation (808 nm).[120] The PEGylated-Ag_2S QDs were proven to be suitable high contrast agents for *in-vivo* video-rate NIR-II fluorescence imaging of 4T1 tumour-bearing Balb/c mice. Interestingly, increasing NIR-II signal intensity was observed in the tumour area in a time-dependent manner post tail-vein injection (Figure 6),[120] and high tumour accumulation of Ag_2S QDs due to the non-specific enhanced permeability and retention (EPR) effect was suggested. The group of H. Dai further presented very encouraging results concerning the *in-vivo* biodistribution of Ag_2S QDs as well as the potential long-term cytotoxic effect. It was found that the PEGylated Ag_2S QDs show main accumulation in the reticular endothelial system (RES) including liver and spleen from where they can be gradually cleared out by excretion. Over a period of 2 months, no significant toxic effect was observed as evidenced by blood biochemistry, haematological analysis and histological examinations.[121]

Among recent research efforts dedicated to the development of bioprobes that exhibit the potential for more specific bioimaging, the work by Li et al., showing the capacity of PEGylated Ag_2S QDs for the diagnosis of circulatory system-related diseases, must be highlighted.[122] As a last but not least example of the most recent cutting-edge research in the field of NIR-to-NIR Ag_2S QDs, the challenge of dynamical tracking of transplanted stem cells *in-vivo* addressed by Chen et al. is worth mentioning.[123] Stem cell tracking is of particular interest with regard to stem cell-based regeneration medicine. In this context, Ag_2S QDs were successfully employed for dynamically *in-vivo* tracking of human mesenchymal stem cells (hMSCs) with high sensitivity and high spatial as well as temporal resolution. Clearly, the progress achieved so far raises high expectations for Ag_2S QDs as alternative and advanced NIR-to-NIR bioprobes for NIR-II imaging.

Lead Chalcogenide QDs

As one of the most recent developments in the field of NIR-to-NIR bioprobes for *in-vivo* imaging, lead (Pb)-based chalcogenides have to be mentioned as highly promising candidates. Like in the case of the other material classes discussed above, efforts to shift the emission of the QDs to the NIR region have focused on materials with shorter energy bandgaps, specifically beyond Cd-based QDs, the workhorse of the last decades. The initial works on colloidal PbSe QDs synthesis by Murray et al. (2001) [124] and on PbS QDs by Hines et al. (2003) [125] brought NIR-II bioimaging within the realm of possibility with these lead chalcogenide systems. Half a decade after these initial works, NIR-II emission under NIR-I excitation of PbS and PbSe QDs was also reported by Hyun et al.[126] Further, the authors firstly demonstrated the potential of mercaptoundecanoic acid (MUA)-capped PbS QDs for cellular NIR-II imaging by recording the 1210 nm emission from the QDs (using the 546 nm line from a mercury lamp for excitation) after incubation with endothelial human colon carcinoma cells (HT29). In 2011, Shuhendler et al. encapsulated PbSe QDs with organic fatty acids, followed by their application as NIR-I-to-NIR-I *in-vivo* bioprobes. It was shown that the encapsulation with organic fatty acids resulted in much lower short-term cytotoxicity compared to non-encapsulated water-dispersible PbSe QDs, reduced liver uptake, increased tumour retention, and nearly complete clearance of the bioprobe from the mouse body. [127] One year later, Won et al. reported the suitability of PbSe QDs for NIR-II bioimaging.[21] The comparative *in-vitro* study of the tissue penetration capability (phantom, porcine skin, and bovine liver tissues) of NIR-I-emitting CdTeSe QDs (800 nm) and NIR-II-emitting PbSe QDs (1300 nm) revealed, once again, the favourable character of NIR-II bioprobes when seeking deep-tissue fluorescence bioimaging. Here, it must be noted that, for comparison reasons, both probes were excited with VIS light (660 nm, required for the excitation of CdTeSe). Yet, the excitation wavelength of PbSe QDs can be shifted into the NIR-I region (850 nm), allowing for further enhancement of the penetration depth.

Regarding the sulphide-based system, Wang et al. reported *in-vivo* NIR-I bioimaging (excitation at 704 nm, emission at 930 nm) using PbS QDs with an SiO_2 shell and PEG capping ligands.[128] Subsequently, the group of T. Jin reported substantial progress on *in-vivo* NIR-II bioimaging using GSH-coated[129] and (EGFP-Protein G)-coated[130] PbS QDs. In the former case, well-resolved NIR-II *ex-vivo* images of breast cancer tumours were recorded upon PbS QDs injection (NIR-I excitation). The second example shows NIR-II fluorescence imaging of a breast tumour at the cellular and whole-body level (VIS (670 nm) excitation). The same group has recently published significant work stressing the advantages of building a CdS shell around the PbS core.[23] Generally speaking, a common challenge when aiming for water-dispersible QDs is the on-going partial loss in luminescence efficiency. The above mentioned work describes the use of MUA as a capping ligand in order to overcome this drawback resulting in improved stability of aqueous PbS/CdS QD dispersions without any severe efficiency loss. Indeed, the QY of the MUA-coated PbS/CdS QDs dispersed in an aqueous buffer solution (PBS) was found to be 17 %, which is significantly higher than that of comparable QDs with other thiol-based capping ligands. This allowed for their successful application in live mouse imaging (Figure 7).

In addition, the Cd-shell approach described above allows for an easier control over the emission wavelength in the 1000 to 1500 nm range, while simultaneously allowing to advantageously work under NIR-I excitation. Applying this strategy, Benayas et al. recently published work reporting NIR-I-to-NIR-II *in-vivo* imaging using PbS/CdS/ZnS QDs. Herein, the outer ZnS shell provides a robust isolation of the heavy-metal core from the environment.[131] In addition, the resultant intense emission from those QDs allowed to substantially decrease the required injection dose when compared to previous reports (two orders of magnitude lower than, for instance, the outstanding Ag_2S bioprobes reported in [120]). This work also offers a preliminary insight into the toxicity of Pb-based nanoprobes. A study was conducted where a mouse injected with PbS/CdS/ZnS QDs was tracked for 25 days and showed no noticeable change in behaviour or weight loss.

Indium-Based QDs as novel NIR-Candidates

This section will provide an overview of the first steps of a new material group that is lately gaining increased interest in the field of NIR-to-NIR bioimaging, namely indium (In)-based QDs. An early report on the *in-vivo* NIR-I-to-NIR-I imaging using InAs core/ZnSe shell QDs, whose water dispersibility was achieved by coating the surface with dihydrolipoic acid conjugated poly(ethylene glycol) (DHLA-PEG), was published in 2005.[132] With the increasing interest in In-based QDs, the investigation of their toxicity becomes an important aspect. Another interesting study by Pons et al. evaluates the potential toxic effects of $CuInS_2$/ZnS QDs as well as their suitability for *in-vivo* NIR-I bioimaging (800 nm emission following 690 nm excitation).[133] The subcutaneous injection of the $CuInS_2$/ZnS QDs in living mice and a subsequent tracking of the lymph node inflammation revealed much lower acute local toxicity than in the case of the reference CdTeSe/CdZnS material. The authors attributed the superior toxicity of CdTeSe/CdZnS QDs to their degradation under *in-vivo* conditions, triggering the release of toxic heavy metal ions such as cadmium and tellurium. Thus, the absence of heavy metal ions is a positive asset for eventual clinical applications of $CuInS_2$/ZnS QDs. While their application as *in-vivo* NIR-II bioprobes is still pending, encouraging *in-vivo* results have been achieved in the NIR-I range. Further interesting In-based nanomaterial platforms were reported in the literature. For instance, achievements concerning the synthesis of InSb QDs

with size-tuneable emission ranging from the NIR-II to the NIR-III region (1200-1750 nm) were reported.[134] Additional promising works report the highly tuneable emissions within the NIR-II range, such as that obtained by CuInP[135] and more lately $AgInS_2$ QDs[136]. This set of binary and ternary In-based QDs can be considered as very promising for future *in-vivo* NIR-to-NIR imaging applications. This is not only based on the ample aforementioned possibilities of tuning their emissions to match with the NIR-II and NIR-III *biological windows*, but also because of their good QY values reportedly ranging between 10 and 20 %. From the toxicity point of view, aside from the preliminary studies mentioned above, it is still far too early to assign any risk scale to this new class of QDs. Although, the lack of heavy metals will likely help to foster further interest in In-based QDs in the forthcoming years within the biomedicine research community.

Novel Organic Dyes for NIR-I and NIR-II Bioimaging

Finally, the following and last section will provide an overview of the first steps of innovative organic dyes as novel probes for NIR-to-NIR bioimaging. A major drawback of conventional organic NIR dyes is the restriction of their imaging range to the 750 to 800 nm wavelength region, which is not optimal due to increased light absorption and scattering when compared to wavelengths longer than 1000 nm. A further challenge is their mostly hydrophobic character leading to aggregation of the dye molecules. This can result in low fluorescence intensities and blue-shift of the absorption peak.[25] Thus, much effort is being undertaken to develop (1) water soluble, non-aggregating organic dyes with enhanced QY and (2) emission wavelengths longer than 1000 nm. Recently, promising probes could be obtained and their suitability for *in-vitro* and *in-vivo* NIR-to-NIR bioimaging was shown as discussed in the following.

Regarding the first challenge, the group of C. Shi focused on the development of novel heptamethine NIR dyes absorbing and emitting in the NIR-I window. Most interestingly, as shown by *in-vivo* NIR-I based imaging, heptamethine dye IR-808 exhibits intrinsic preferential tumour accumulation and photosensitizing activities without the need of chemical conjugation with tumour specific ligands and photosensitizers. Moreover, treatment of tumour bearing mice with IR-808 under irradiation showed significant suppression of tumour growth making this NIR-I dye also a promising candidate for photodynamic therapy.[137] The light-mediated cytotoxic effect could be further enhanced by chemical modification of IR-808 (referred to as IR-808DB dye) providing NIR-I cancer-targeted imaging and potent anticancer activity.[138] In a different approach, Chuo et al. doped polymer nanoparticles (polyethylene glycol-conjugated phospholipid DSPE-$mPEG_{5000}$) with the dye IR-820 (excitation at 635 nm, emission at 820 nm) and demonstrated their suitability for macro and microscopic *in-vivo* imaging. Macroscopic biodistribution studies revealed that the doped nanoparticles were excreted from the mouse body through its hepatobiliary transport and that they showed very little toxicity, which may facilitate their biomedical application. Moreover, the NIR-I emitting IR-820 doped polymer nanoparticles allowed for *in-vivo* microscopic imaging of blood vessels in a mouse ear as well as blood vasculature in a mouse brain.[139] The concept of combining a polymer nanoparticle with a NIR fluorescent molecule was also followed by Lv et al.[140] In this work, the conjugated polymer P-F8-DPSB, which exhibits two-photon excited fluorescence (TPEF), was used as the NIR-light harvesting component and the energy donor, while a NIR fluorescent dye (DPA-PR-PDI) was used as the energy acceptor and the NIR-light emitting component. The obtained hybrid nanoparticles revealed a QY of up to 45 %, and NIR-I *in-vitro* imaging of HeLa cells through mock tissue of up to 900 μm thickness was demonstrated (excitation: 800 nm, emission: 730 nm).

Finally, seeking novel probes for bioimaging in the wavelength region above 1000 nm, recent work by the group of H. Dai must be highlighted. In 2013, the authors reported the first biocompatible organic NIR-II agent for *in-vivo* imaging. In their approach, the water insoluble commercial dye IR-1061 was embedded in the amphiphilic polymer PAA and subsequently coated with the surfactant DSPE-mPEG providing water solubility. By use of these probes, the first NIR-II imaging of inner organs and blood vessels of mice with organic molecular fluorophores (excitation at 808 nm) could be demonstrated.[141] In 2014, the same group presented an organic fluorophore that brightly (QY ~ 1.7 %) emits in the NIR-II region from 1050 to 1350 nm obtained by copolymerization of an electron-donating monomer (benzo[1,2-b:3,4-b´]difuran) and an electron-withdrawing monomer (fluorothieno-[3,4-b]thiophene).[142] PEG-modification of the polymer provided the water solubility and biocompatibility necessary for *in-vivo* applications. The high temporal resolution of the obtained organic NIR-II bioprobes allowed for the *in-vivo* observation of the rapid periodic oscillation in the femoral blood velocity in mice (Figure 8). Such video-rate imaging of dynamic changes in the blood flow is of particular interest since it could be of central importance to better understand various cardiovascular diseases and to design novel therapy approaches. Obviously, these developments in the field of organic NIR-II dyes are highly encouraging with respect to future achievements in the field of NIR-to-NIR bioimaging using organic dyes.

Conclusions

Summarizing the results and findings from globally conducted research studies on deep-tissue optical bioimaging, the NIR region that overlaps with the three *biological windows* (700-1870 mm) has clearly been identified as the wavelength region of choice that should replace commonly used UV-VIS light. In fact, the increasing attraction of NIR-based optical bioimaging

has been in unison with the availability of suitable and affordable NIR-detection systems. This logically triggers the need for the development of bright NIR-emitting bioprobes. Further constraints that need to be overcome include stable dispersibility in aqueous biological media, chemical and physical stability under biological conditions, biocompatibility, and the ability for specific imaging. In the search for candidates that combine these optical and biological requirements, choices span the gamut from organic dyes to inorganic nanoparticles and QDs. However, independent of the chosen material, a major consensus has been reached regarding the optimal emission wavelength, namely wavelengths longer than 1000 nm. Upon inspection of the various material classes that are at the forefront of recent developments, RE^{3+}-doped nanoparticles have proven to be versatile NIR-emitters since the choice of the RE^{3+} dopant allows for the adjustment of both, excitation (NIR-I) and emission (NIR-II and III) wavelengths. Moreover, RE^{3+}-based nanoparticles are promising for biomedical applications due to their reported biocompatibility as well as their potential as multifunctional theranostic probes. Particularly with regard to high-resolution, SWCNTs provide one of the most promising systems allowing for high spatial and temporal resolution. Yet, their potential toxicity is a major concern that needs to be addressed in order to be safely used in biomedical applications. Besides the urge to clarify and overcome toxicity aspects, societal perceptions must also be taken into account given their rigid needle-like structure that draws parallels with pathogenic asbestos. A similar challenge concerning societal perception is facing the Pb-based class of QDs due to their heavy metal content even though recent applications as NIR-to-NIR bioprobes are highly promising. In the context of QDs, the rather novel material class of Ag chalcogenides reveals encouraging toxicity results, and recent reports on their NIR-II *in-vitro* and *in-vivo* bioimaging raise expectations about future developments. Following this trend in innovative, non-toxic probes for NIR-to-NIR bioimaging, CNPs as well as In-, Si, and Ge-based nanostructures are receiving increasing interest. First *in-vitro* and *in-vivo* studies were reported for CNPs, In- and Si-based NIR-emitters, while the development of NIR-emitting Ge NCs is at an even earlier research stage. Organic dyes that emit at wavelengths longer than 1000 nm are still very scarce. Yet, the first *in-vivo* bioimaging results in the NIR-II window were recently reported and expectations continue to rise concerning innovative future organic NIR-to-NIR probes.

Overall, while each material class has its own challenges that must be overcome through on-going interdisciplinary research, very promising work has already been published (Scheme 2) that allows us to glance optimistically at the future of NIR-to-NIR deep-tissue bioimaging.

Acknowledgements

E. Hemmer is thankful to the Alexander von Humboldt Foundation for financial support in the frame of the Feodor Lynen Research Fellowship. A. Benayas thanks the Canadian Institutes of Health Research and the Breast Cancer Society of Canada (CIHR-BCSC), for postdoctoral funding granted to him through an Eileen Iwanicki Fellowship in Breast Cancer Imaging. F. Légaré and F. Vetrone are thankful to the Natural Sciences and Engineering Research Council of Canada (NSERC) and the Fonds de recherche du Québec – Nature et technologies (FRQNT) for supporting their research programmes.

Notes and references

1. E. M. C. Hillman, C. B. Amoozegar, T. Wang, A. F. H. McCaslin, M. B. Bouchard, J. Mansfield and R. M. Levenson, *Philos. Trans. R. Soc. A-Math. Phys. Eng. Sci.,* 2011, **369**, 4620-4643.
2. X. X. He, J. H. Gao, S. S. Gambhir and Z. Cheng, *Trends Mol. Med.,* 2010, **16**, 574-583.
3. R. R. Anderson and J. A. Parrish, *J. Invest. Dermatol.,* 1981, **77**, 13-19.
4. A. M. Smith, M. C. Mancini and S. Nie, *Nat. Nanotechnol.,* 2009, **4**, 710-711.
5. L. A. Sordillo, Y. Pu, S. Pratavieira, Y. Budansky and R. R. Alfano, *J. Biomed. Opt.,* 2014, **19**, 056004.
6. L. Prodi, E. Rampazzo, F. Rastrelli, A. Speghini and N. Zaccheroni, *Chem. Soc. Rev.,* 2015, **44**, 4922-4952.
7. M. Fox, *Optical Properties of Solids*. Oxford University Press: Oxford, 2001.
8. T. Durduran, R. Choe, W. B. Baker and A. G. Yodh, *Rep. Prog. Phys.,* 2010, **73**, 076701.
9. A. N. Bashkatov, E. A. Genina, V. I. Kochubey and V. V. Tuchin, *J. Phys. D-Appl. Phys.,* 2005, **38**, 2543-2555.
10. S. L. Jacques, *Phys. Med. Biol.,* 2013, **58**, R37-R61.
11. S. Diao, G. Hong, A. L. Antaris, J. L. Blackburn, K. Cheng, Z. Cheng and H. Dai, *Nano Res.,* 2015, **8**, 3027-3034.
12. R. C. Benson and H. A. Kues, *Phys. Med. Biol.,* 1978, **23**, 159-163.
13. R. Philip, A. Penzkofer, W. Baumler, R. M. Szeimies and C. Abels, *J. Photochem. Photobiol. A-Chem.,* 1996, **96**, 137-148.
14. S. Luo, E. Zhang, Y. Su, T. Cheng and C. Shi, *Biomaterials,* 2011, **32**, 7127-7138.
15. J. O. Escobedo, O. Rusin, S. Lim and R. M. Strongin, *Curr. Opin. Chem. Biol.,* 2010, **14**, 64-70.
16. X. Michalet, F. F. Pinaud, L. A. Bentolila, J. M. Tsay, S. Doose, J. J. Li, G. Sundaresan, A. M. Wu, S. S. Gambhir and S. Weiss, *Science,* 2005, **307**, 538-544.
17. W. B. Cai, A. R. Hsu, Z. B. Li and X. Y. Chen, *Nanoscale Res. Lett.,* 2007, **2**, 265-281.
18. R. G. Aswathy, Y. Yoshida, T. Maekawa and D. S. Kumar, *Anal. Bioanal. Chem.,* 2010, **397**, 1417-1435.
19. P. Wu and X. P. Yan, *Chem. Soc. Rev.,* 2013, **42**, 5489-5521.
20. L. Chen and H. Y. Han, *Microchim. Acta,* 2014, **181**, 1485-1495.
21. N. Won, S. Jeong, K. Kim, J. Kwag, J. Park, S. G. Kim and S. Kim, *Mol. Imaging,* 2012, **11**, 338-352.

22. X. Y. Ji, F. Peng, Y. L. Zhong, Y. Y. Su and Y. He, *Colloid Surf. B-Biointerfaces,* 2014, **124**, 132-139.
23. Y. Tsukasaki, M. Morimatsu, G. Nishimura, T. Sakata, H. Yasuda, A. Komatsuzaki, T. M. Watanabe and T. Jin, *RSC Adv.,* 2014, **4**, 41164-41171.
24. X. W. He and N. Ma, *Colloid Surf. B-Biointerfaces,* 2014, **124**, 118-131.
25. C. L. Amiot, S. Xu, S. Liang, L. Pan and J. X. Zhao, *Sensors,* 2008, **8**, 3082-3105.
26. M. A. Hahn, A. K. Singh, P. Sharma, S. C. Brown and B. M. Moudgil, *Anal. Bioanal. Chem.,* 2011, **399**, 3-27.
27. E. Cassette, M. Helle, L. Bezdetnaya, F. Marchal, B. Dubertret and T. Pons, *Adv. Drug Deliv. Rev.,* 2013, **65**, 719-731.
28. J. Yao, M. Yang and Y. X. Duan, *Chem. Rev.,* 2014, **114**, 6130-6178.
29. Z. Li, Q. Sun, Y. Zhu, B. Tan, Z. P. Xu and S. X. Dou, *J. Mat. Chem. B,* 2014, **2**, 2793-2818.
30. J. Pichaandi and F. C. J. M. van Veggel, *Coord. Chem. Rev.,* 2014, **263**, 138-150.
31. H. S. Peng and D. T. Chiu, *Chem. Soc. Rev.,* 2015, **44**, 4699-4722.
32. O. S. Wolfbeis, *Chem. Soc. Rev.,* 2015, **44**, 4743-4768.
33. J. C. G. Bunzli, S. Comby, A. S. Chauvin and C. D. B. Vandevyver, *J. Rare Earths,* 2007, **25**, 257-274.
34. R. Naccache, Q. Yu and J. A. Capobianco, *Adv. Opt. Mater.,* 2015, **3**, 482-509.
35. G. Y. Chen, C. H. Yang and P. N. Prasad, *Accounts Chem. Res.,* 2013, **46**, 1474-1486.
36. S. L. Gai, C. X. Li, P. P. Yang and J. Lin, *Chem. Rev.,* 2014, **114**, 2343-2389.
37. F. C. J. M. van Veggel, *Chem. Mater.,* 2014, **26**, 111-122.
38. B. Somogyi, V. Zolyomi and A. Gali, *Nanoscale,* 2012, **4**, 7720-6.
39. E. Borsella, R. D'Amato, M. Falconieri, E. Trave, A. Panariti and I. Rivolta, *J. Mater. Res.,* 2012, **28**, 193-204.
40. J. Fan and P. K. Chu, *Small,* 2010, **6**, 2080-98.
41. L. M. Lacroix, F. Delpech, C. Nayral, S. Lachaize and B. Chaudret, *Interface Focus,* 2013, **3**, 20120103.
42. Y. Miyauchi, M. Iwamura, S. Mouri, T. Kawazoe, M. Ohtsu and K. Matsuda, *Nat. Photonics,* 2013, **7**, 715-719.
43. M. J. O'Connell, S. M. Bachilo, C. B. Huffman, V. C. Moore, M. S. Strano, E. H. Haroz, K. L. Rialon, P. J. Boul, W. H. Noon, C. Kittrell, J. P. Ma, R. H. Hauge, R. B. Weisman and R. E. Smalley, *Science,* 2002, **297**, 593-596.
44. A. Jain, A. Homayoun, C. W. Bannister and K. Yum, *Biotechnol. J.,* 2015, **10**, 447-459.
45. S. Cotton, *Lanthanide and Actinide Chemistry*. John Wiley & Sons Ltd: Chichester, 2006.
46. M. Nyk, R. Kumar, T. Y. Ohulchanskyy, E. J. Bergey and P. N. Prasad, *Nano Lett.,* 2008, **8**, 3834-3838.
47. J. Zhou, Y. Sun, X. Du, L. Xiong, H. Hu and F. Li, *Biomaterials,* 2010, **31**, 3287-95.
48. J. C. Zhou, Z. L. Yang, W. Dong, R. J. Tang, L. D. Sun and C. H. Yan, *Biomaterials,* 2011, **32**, 9059-67.
49. T. S. Yang, Y. Sun, Q. Liu, W. Feng, P. Y. Yang and F. Y. Li, *Biomaterials,* 2012, **33**, 3733-3742.
50. M. Kamimura, N. Kanayama, K. Tokuzen, K. Soga and Y. Nagasaki, *Nanoscale,* 2011, **3**, 3705-13.
51. E. Hemmer, N. Venkatachalam, H. Hyodo, A. Hattori, Y. Ebina, H. Kishimoto and K. Soga, *Nanoscale,* 2013, **5**, 11339-11361.
52. E. Hemmer, F. Vetrone and K. Soga, *MRS Bull.,* 2014, **39**, 960-964.
53. A. Gnach, T. Lipinski, A. Bednarkiewicz, J. Rybka and J. A. Capobianco, *Chem. Soc. Rev.,* 2015, **44**, 1561-1584.
54. E. Hemmer, T. Yamano, H. Kishimoto, N. Venkatachalam, H. Hyodo and K. Soga, *Acta Biomater.,* 2013, **9**, 4734-4743.
55. N. Venkatachalam, E. Hemmer, T. Yamano, H. Hyodo, H. Kishimoto and K. Soga, *Prog. Cryst. Growth Charact. Mater.,* 2012, **58**, 121-134.
56. L. Cheng, K. Yang, M. W. Shao, X. H. Lu and Z. Liu, *Nanomed.: Nanotechnol. Biol. Med.,* 2011, **6**, 1327-1340.
57. L. Q. Xiong, T. S. Yang, Y. Yang, C. J. Xu and F. Y. Li, *Biomaterials,* 2010, **31**, 7078-7085.
58. D. M. Yang, P. A. Ma, Z. Y. Hou, Z. Y. Cheng, C. X. Li and J. Lin, *Chem. Soc. Rev.,* 2015, **44**, 1416-1448.
59. D. Jaque and F. Vetrone, *Nanoscale,* 2012, **4**, 4301-4326.
60. X. Wu, G. Y. Chen, J. Shen, Z. J. Li, Y. W. Zhang and G. Han, *Bioconjug. Chem.,* 2015, **26**, 166-175.
61. Z. Chen, W. Zheng, P. Huang, D. T. Tu, S. Y. Zhou, M. D. Huang and X. Y. Chen, *Nanoscale,* 2015, **7**, 4274-4290.
62. E. Hemmer, H. Takeshita, T. Yamano, T. Fujiki, Y. Kohl, K. Löw, N. Venkatachalam, H. Hyodo, H. Kishimoto and K. Soga, *J. Mater. Sci.-Mater. Med.,* 2012, **23**, 2399-2412.
63. N. Venkatachalam, T. Yamano, E. Hemmer, H. Hyodo, H. Kishimoto and K. Soga, *J. Am. Ceram. Soc.,* 2013, **96**, 2759-2765.
64. T. Zako, M. Yoshimoto, H. Hyodo, H. Kishimoto, M. Ito, K. Kaneko, K. Soga and M. Maeda, *Biomater. Sci.,* 2015, **3**, 59-64.
65. D. J. Naczynski, M. C. Tan, M. Zevon, B. Wall, J. Kohl, A. Kulesa, S. Chen, C. M. Roth, R. E. Riman and P. V. Moghe, *Nat. Commun.,* 2013, **4**, 2199.
66. R. Wang, X. M. Li, L. Zhou and F. Zhang, *Angew. Chem. Int. Edit.,* 2014, **53**, 12086-12090.
67. G. Y. Chen, T. Y. Ohulchanskyy, S. Liu, W. C. Law, F. Wu, M. T. Swihart, H. Agren and P. N. Prasad, *ACS Nano,* 2012, **6**, 2969-2977.
68. M. Pokhrel, L. C. Mimun, B. Yust, G. A. Kumar, A. Dhanale, L. Tang and D. K. Sardar, *Nanoscale,* 2014, **6**, 1667-1674.
69. I. Villa, A. Vedda, I. X. Cantarelli, M. Pedroni, F. Piccinelli, M. Bettinelli, A. Speghini, M. Quintanilla, F. Vetrone, U. Rocha, C. Jacinto, E. Carrasco, F. S. Rodriguez, A. Juarranz, B. del Rosal, D. H. Ortgies, P. H. Gonzalez, J. G. Sole and D. J. Garcia, *Nano Res.,* 2015, **8**, 649-665.
70. U. Rocha, K. U. Kumar, C. Jacinto, I. Villa, F. Sanz-Rodriguez, M. D. I. de la Cruz, A. Juarranz, E. Carrasco, F. C. J. M. van Veggel, E. Bovero, J. G. Sole and D. Jaque, *Small,* 2014, **10**, 1141-1154.
71. U. Rocha, K. U. Kumar, C. Jacinto, J. Ramiro, A. J. Caamano, J. G. Sole and D. Jaque, *Appl. Phys. Lett.,* 2014, **104**, 053703.
72. E. Carrasco, B. del Rosal, F. Sanz-Rodriguez, A. J. de la Fuente, P. H. Gonzalez, U. Rocha, K. U. Kumar, C. Jacinto, J. G. Sole and D. Jaque, *Adv. Funct. Mater.,* 2015, **25**, 615-626.
73. R. W. Y. Habash, R. Bansal, D. Krewski and H. T. Alhafid, *Crit. Rev. Biomed. Eng.,* 2006, **34**, 459-89.
74. J. C. G. Esteves da Silva and H. M. R. Gonçalves, *TRAC Trends Anal. Chem.,* 2011, **30**, 1327-1336.
75. J. Shen, Y. Zhu, X. Yang and C. Li, *Chem. Commun.,* 2012, **48**, 3686-99.
76. X. Wu, F. Tian, W. Wang, J. Chen, M. Wu and J. X. Zhao, *Journal of materials chemistry. C, Materials for optical and electronic devices,* 2013, **1**, 4676-4684.

77. H. Yan, M. Tan, D. Zhang, F. Cheng, H. Wu, M. Fan, X. Ma and J. Wang, *Talanta,* 2013, **108**, 59-65.
78. L. Wu, M. Luderer, X. Yang, C. Swain, H. Zhang, K. Nelson, A. J. Stacy, B. Shen, G. M. Lanza and D. Pan, *Theranostics,* 2013, **3**, 677-86.
79. M. Foldvari and M. Bagonluri, *Nanomed. - Nanotechnol. Biol. Med.,* 2008, **4**, 183-200.
80. Z. Liu, S. Tabakman, K. Welsher and H. J. Dai, *Nano Res.,* 2009, **2**, 85-120.
81. Z. Liu, J. T. Robinson, S. M. Tabakman, K. Yang and H. J. Dai, *Mater. Today,* 2011, **14**, 316-323.
82. J. H. Ahn, J. H. Kim, N. F. Reuel, P. W. Barone, A. A. Boghossian, J. Q. Zhang, H. Yoon, A. C. Chang, A. J. Hilmer and M. S. Strano, *Nano Lett.,* 2011, **11**, 2743-2752.
83. R. Singh and S. V. Torti, *Adv. Drug Deliv. Rev.,* 2013, **65**, 2045-2060.
84. H. Huang, M. Zou, X. Xu, F. Liu, N. Li and X. Wang, *TRAC Trends Anal. Chem.,* 2011, **30**, 1109-1119.
85. P. Cherukuri, S. M. Bachilo, S. H. Litovsky and R. B. Weisman, *J. Am. Chem. Soc.,* 2004, **126**, 15638-15639.
86. K. Welsher, Z. Liu, D. Daranciang and H. Dai, *Nano Lett.,* 2008, **8**, 586-590.
87. J. H. Choi, F. T. Nguyen, P. W. Barone, D. A. Heller, A. E. Moll, D. Patel, S. A. Boppart and M. S. Strano, *Nano Lett.,* 2007, **7**, 861-867.
88. K. Welsher, S. P. Sherlock and H. Dai, *Proc. Natl. Acad. Sci. USA,* 2011, **108**, 8943-8.
89. K. Welsher, Z. Liu, S. P. Sherlock, J. T. Robinson, Z. Chen, D. Daranciang and H. J. Dai, *Nat. Nanotechnol.,* 2009, **4**, 773-780.
90. J. T. Robinson, G. S. Hong, Y. Y. Liang, B. Zhang, O. K. Yaghi and H. J. Dai, *J. Am. Chem. Soc.,* 2012, **134**, 10664-10669.
91. G. S. Hong, J. C. Lee, J. T. Robinson, U. Raaz, L. M. Xie, N. F. Huang, J. P. Cooke and H. J. Dai, *Nat. Med.,* 2012, **18**, 1841-1846.
92. G. S. Hong, S. Diao, J. L. Chang, A. L. Antaris, C. X. Chen, B. Zhang, S. Zhao, D. N. Atochin, P. L. Huang, K. I. Andreasson, C. J. Kuo and H. J. Dai, *Nat. Photonics,* 2014, **8**, 723-730.
93. Y. Song, X. Li and X. Du, *Eur. Resp. J.,* 2009, **34**, 559-567.
94. M. Pacurari, V. Castranova and V. Vallyathan, *J. Toxicol. Env. Health Part A,* 2010, **73**, 378-395.
95. Y. Rodriguez-Yanez, B. Munoz and A. Albores, *Toxicol. Mech. Methods,* 2013, **23**, 178-195.
96. S. Toyokuni, *Adv. Drug Deliv. Rev.,* 2013, **65**, 2098-2110.
97. M. L. Becker, J. A. Fagan, N. D. Gallant, B. J. Bauer, V. Bajpai, E. K. Hobbie, S. H. Lacerda, K. B. Migler and J. P. Jakupciak, *Adv. Mater.,* 2007, **19**, 939-945.
98. V. Castranova, P. A. Schulte and R. D. Zumwalde, *Accounts Chem. Res.,* 2013, **46**, 642-649.
99. P. Moller, D. V. Christophersen, D. M. Jensen, A. Kermanizadeh, M. Roursgaard, N. R. Jacobsen, J. G. Hemmingsen, P. H. Danielsen, Y. Cao, K. Jantzen, H. Klingberg, L. G. Hersoug and S. Loft, *Arch. Toxicol.,* 2014, **88**, 1939-1964.
100. C. Bussy, L. Methven and K. Kostarelos, *Adv. Drug Deliv. Rev.,* 2013, **65**, 2127-2134.
101. S. Bhattacharjee, I. M. Rietjens, M. P. Singh, T. M. Atkins, T. K. Purkait, Z. Xu, S. Regli, A. Shukaliak, R. J. Clark, B. S. Mitchell, G. M. Alink, A. T. Marcelis, M. J. Fink, J. G. Veinot, S. M. Kauzlarich and H. Zuilhof, *Nanoscale,* 2013, **5**, 4870-83.
102. J. H. Park, L. Gu, G. von Maltzahn, E. Ruoslahti, S. N. Bhatia and M. J. Sailor, *Nat. Mater.,* 2009, **8**, 331-6.
103. S. Chinnathambi, S. Chen, S. Ganesan and N. Hanagata, *Adv. Healthc. Mater.,* 2014, **3**, 10-29.
104. B. F. P. McVey and R. D. Tilley, *Accounts Chem. Res.,* 2014, **47**, 3045-3051.
105. M. Falconieri, R. D'Amato, F. Fabbri, M. Carpanese and E. Borsella, *Physica E: Low-dim. Syst. Nanostruct.,* 2009, **41**, 951-954.
106. E. J. Henderson, A. J. Shuhendler, P. Prasad, V. Baumann, F. Maier-Flaig, D. O. Faulkner, U. Lemmer, X. Y. Wu and G. A. Ozin, *Small,* 2011, **7**, 2507-16.
107. G. S. He, Q. D. Zheng, K. T. Yong, F. Erogbogbo, M. T. Swihart and P. N. Prasad, *Nano Lett.,* 2008, **8**, 2688-2692.
108. D. C. Lee, J. M. Pietryga, I. Robel, D. J. Werder, R. D. Schaller and V. I. Klimov, *J. Am. Chem. Soc.,* 2009, **131**, 3436-3437.
109. D. A. Ruddy, J. C. Johnson, E. R. Smith and N. R. Neale, *ACS Nano,* 2010, **4**, 7459-7466.
110. Y. H. Ma, C. P. Huang, J. S. Tsai, M. Y. Shen, Y. K. Li and L. Y. Lin, *Toxicol. Lett.,* 2011, **207**, 258-69.
111. A. Karatutlu, M. Y. Song, A. P. Wheeler, O. Ersoy, W. R. Little, Y. P. Zhang, P. Puech, F. S. Boi, Z. Luklinska and A. V. Sapelkin, *RSC Adv.,* 2015, **5**, 20566-20573.
112. R. Gui, H. Jin, Z. Wang and L. Tan, *Coord. Chem. Rev.,* 2015, **296**, 91-124.
113. Y. X. Zhao and Z. M. Song, *Materials Letters,* 2014, **126**, 78-80.
114. H. Y. Yang, Y. W. Zhao, Z. Y. Zhang, H. M. Xiong and S. N. Yu, *Nanotechnology,* 2013, **24**, 055706.
115. R. J. Gui, A. J. Wan, X. F. Liu, W. Yuan and H. Jin, *Nanoscale,* 2014, **6**, 5467-5473.
116. R. J. Gui, J. Sun, D. X. Liu, Y. F. Wang and H. Jin, *Dalton Trans.,* 2014, **43**, 16690-16697.
117. Y. Zhang, G. S. Hong, Y. J. Zhang, G. C. Chen, F. Li, H. J. Dai and Q. B. Wang, *ACS Nano,* 2012, **6**, 3695-3702.
118. L. J. Tan, A. Wan and H. L. Li, *Langmuir,* 2013, **29**, 15032-15042.
119. L. J. Tan, A. J. Wan and H. L. Li, *ACS applied materials & interfaces,* 2014, **6**, 18-23.
120. G. Hong, J. T. Robinson, Y. Zhang, S. Diao, A. L. Antaris, Q. Wang and H. Dai, *Angew. Chem. Int. Edit.,* 2012, **51**, 9818-21.
121. Y. Zhang, Y. J. Zhang, G. S. Hong, W. He, K. Zhou, K. Yang, F. Li, G. C. Chen, Z. Liu, H. J. Dai and Q. B. Wang, *Biomaterials,* 2013, **34**, 3639-3646.
122. C. Y. Li, Y. J. Zhang, M. Wang, Y. Zhang, G. C. Chen, L. Li, D. M. Wu and Q. B. Wang, *Biomaterials,* 2014, **35**, 393-400.
123. G. C. Chen, F. Tian, Y. Zhang, Y. J. Zhang, C. Y. Li and Q. B. Wang, *Adv. Funct. Mater.,* 2014, **24**, 2481-2488.
124. C. B. Murray, S. H. Sun, W. Gaschler, H. Doyle, T. A. Betley and C. R. Kagan, *IBM J. Res. Dev.,* 2001, **45**, 47-56.
125. M. A. Hines and G. D. Scholes, *Adv. Mater.,* 2003, **15**, 1844-1849.
126. B. R. Hyun, H. Y. Chen, D. A. Rey, F. W. Wise and C. A. Batt, *J. Phys. Chem. B,* 2007, **111**, 5726-5730.
127. A. J. Shuhendler, P. Prasad, H. K. C. Chan, C. R. Gordijo, B. Soroushian, M. Kolios, K. Yu, P. J. O'Brien, A. M. Rauth and X. Y. Wu, *ACS Nano,* 2011, **5**, 1958-1966.
128. D. Wang, J. Qian, F. Cai, S. He, S. Han and Y. Mu, *Nanotechnology,* 2012, **23**, 245701.
129. Y. Nakane, Y. Tsukasaki, T. Sakata, H. Yasuda and T. Jin, *Chem. Commun.,* 2013, **49**, 7584-7586.

130. A. Sasaki, Y. Tsukasaki, A. Komatsuzaki, T. Sakata, H. Yasuda and T. Jin, *Nanoscale,* 2015, **7**, 5115-5119.
131. A. Benayas, F. Ren, E. Carrasco, V. Marzal, B. del Rosal, B. Gonfa, A. Juarranz, F. Sanz-Rodríguez, D. Jaque, J. García Solé, D. Ma and F. Vetrone, *Adv. Funct. Mater.,* 2015, **25**, 6650–6659.
132. J. P. Zimmer, S. W. Kim, S. Ohnishi, E. Tanaka, J. V. Frangioni and M. G. Bawendi, *J. Am. Chem. Soc.,* 2006, **128**, 2526-2527.
133. T. Pons, E. Pic, N. Lequeux, E. Cassette, L. Bezdetnaya, F. Guillemin, F. Marchal and B. Dubertret, *ACS Nano,* 2010, **4**, 2531-2538.
134. W. Y. Liu, A. Y. Chang, R. D. Schaller and D. V. Talapin, *J. Am. Chem. Soc.,* 2012, **134**, 20258-20261.
135. R. G. Xie and X. G. Peng, *J. Am. Chem. Soc.,* 2009, **131**, 10645-10651.
136. M. A. Langevin, A. M. Ritcey and C. Ni Allen, *ACS Nano,* 2014, **8**, 3476-3482.
137. X. Tan, S. L. Luo, D. C. Wang, Y. P. Su, T. M. Cheng and C. M. Shi, *Biomaterials,* 2012, **33**, 2230-2239.
138. S. L. Luo, X. Tan, Q. R. Qi, Q. Y. Guo, X. Z. Ran, L. L. Zhang, E. L. Zhang, Y. F. Liang, L. L. Weng, H. Zheng, T. M. Cheng, Y. P. Su and C. M. Shi, *Biomaterials,* 2013, **34**, 2244-2251.
139. L. L. Chu, S. W. Wang, K. H. Li, W. Xi, X. Y. Zhao and J. Qian, *Biomed. Opt. Express,* 2014, **5**, 4076-4088.
140. Y. L. Lv, P. Liu, H. Ding, Y. S. Wu, Y. L. Yan, H. Liu, X. F. Wang, F. Huang, Y. S. Zhao and Z. Y. Tian, *ACS Appl. Mater. Interfaces,* 2015, **7**, 20640-20648.
141. Z. M. Tao, G. S. Hong, C. Shinji, C. X. Chen, S. Diao, A. L. Antaris, B. Zhang, Y. P. Zou and H. J. Dai, *Angew. Chem. Int. Edit.,* 2013, **52**, 13002-13006.
142. G. S. Hong, Y. P. Zou, A. L. Antaris, S. Diao, D. Wu, K. Cheng, X. D. Zhang, C. X. Chen, B. Liu, Y. H. He, J. Z. Wu, J. Yuan, B. Zhang, Z. M. Tao, C. Fukunaga and H. J. Dai, *Nat. Commun.,* 2014, **5**, 4206.

Journal Name

ARTICLE

FIGURES AND SCHEMES

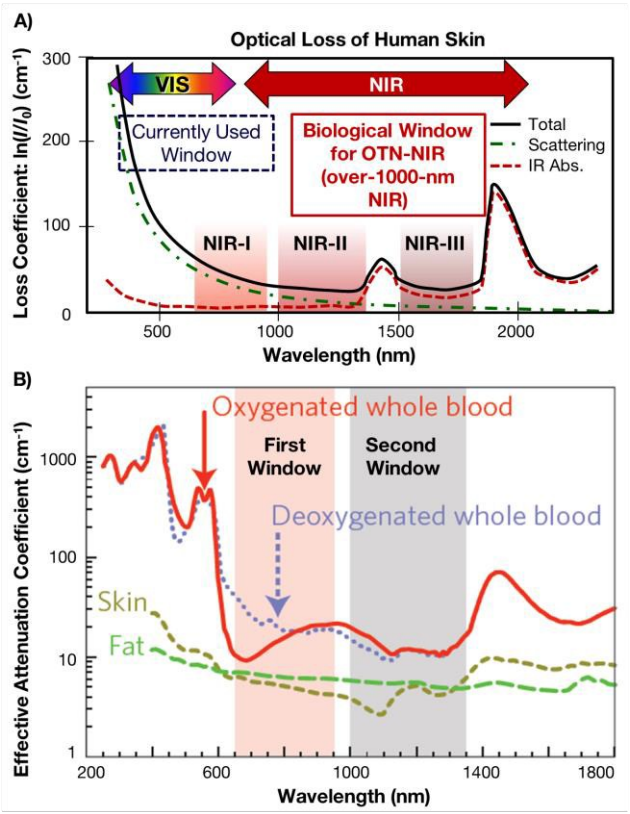

Figure 1. A) Absorption spectrum of human skin showing the first (NIR-I), second (NIR-II) and third (NIR-III) *biological windows*. Reproduced from reference [51] with permission from The Royal Society of Chemistry. B) Zoom-in of the two first optical windows in some biological tissues and fluids. These plots of effective attenuation coefficient (on a log scale) versus wavelength show the quantitative relevance of different body substances (oxygenated blood, deoxygenated blood, skin and fatty tissue) when aiming for deep sub-skin imaging.[4] Reprinted by permission from Macmillan Publishers Ltd: Nature Nanotechnol., 2009, 4, 710-711. Copyright (2009).

(SINGLE COLUMN, 8.3cm)

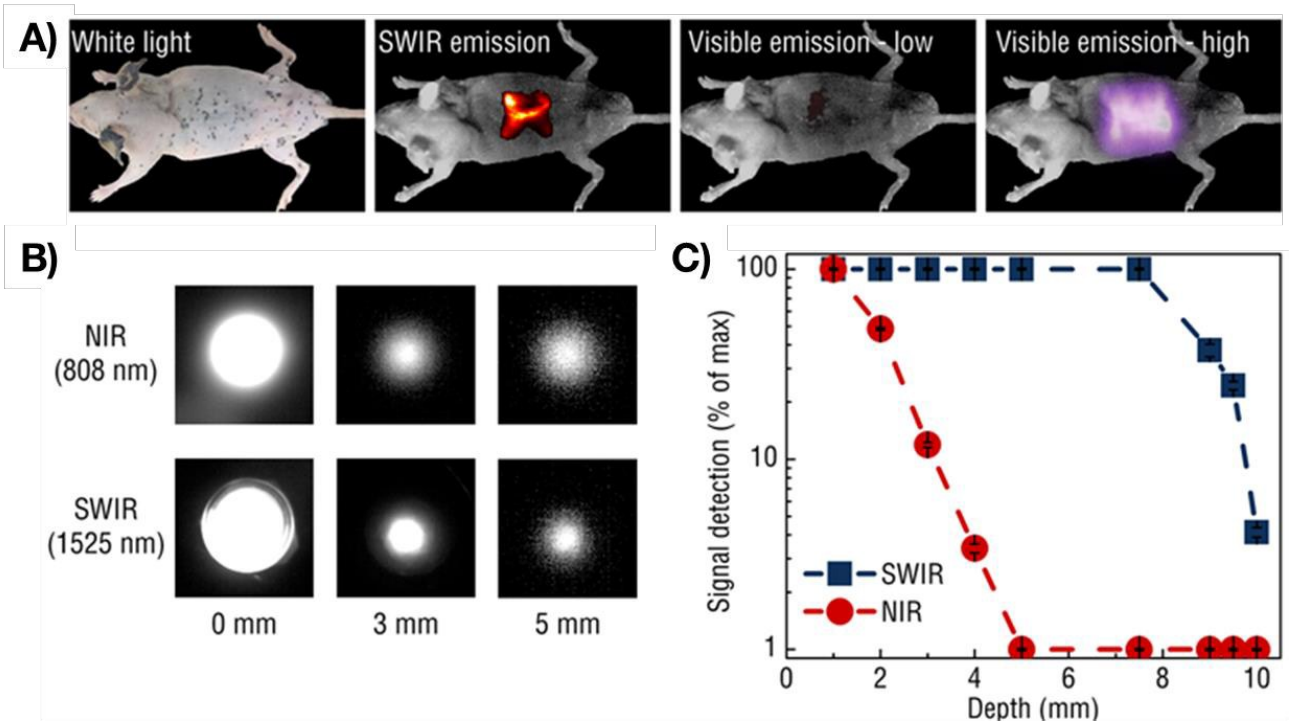

Figure 2. Demonstration of the imaging advantages by use of NIR-III (SWIR: defined by the authors as short wavelength infrared light, 1000-2300 nm) light compared to VIS or NIR-I (NIR: defined by the authors as near infrared light, 700-1000 nm). A) A pattern in the shape of an "R" using Er^{3+}/Yb^{3+}:$NaYF_4$ core / $NaYF_4$ shell nanoparticles under 980 nm excitation (laser power: 0.14 W cm^{-2}) can be seen clearly through a mouse body with resected intestines, which is not possible for VIS light. Increase of the excitation power to 0.5 W cm^{-2} results in a detectable VIS signal, however at much lower resolution when compared to NIR-III (SWIR). B) Influence of the emission wavelength on the achievable penetration depth. A more distinct signal at increased phantom tissue thickness is obtained for NIR-III (SWIR) compared to NIR-I (NIR). C) Detectable signals as a function of phantom tissue thickness for NIR-III (SWIR) and NIR-I (NIR) emission revealing improved light propagation in case of NIR-III (SWIR, blue data points).[65] Reprinted by permission from Macmillan Publishers Ltd: *Nature Comm.*, 2013, 4, 2199 (10 pp). Copyright (2013).

(DOUBLE COLUMN, 17.1cm)

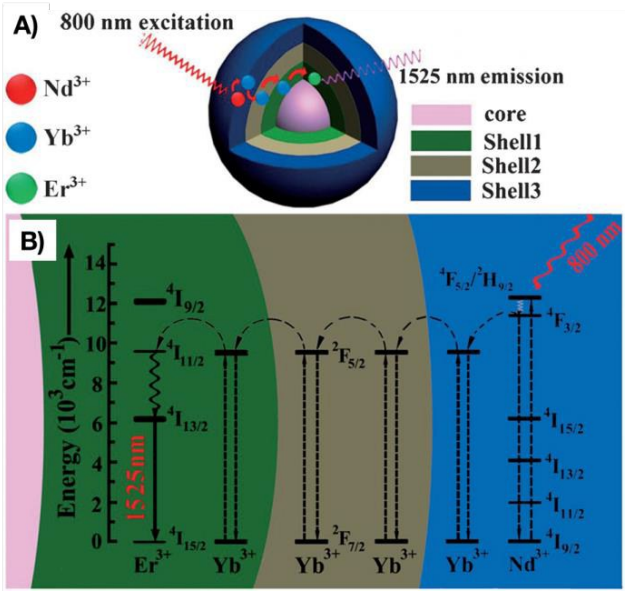

Scheme 1. Optimization of the excitation and emission wavelength through a complex RE^{3+}-based core/multishell nanostructure composed by A) a $NaGdF_4$ core, a first Er^{3+}:Na(Gd,Yb)F_4 shell, an intermediate Yb^{3+}:$NaYF_4$ shell, and an outer Yb^{3+}:$NaNdF_4$ shell. B) Proposed energy transfer mechanism allowing for NIR-III emission (1525 nm) from Er^{3+} after NIR-I (800 nm) excitation of Nd^{3+}. From reference [66] with permission from John Wiley and Sons.

(SINGLE COLUMN, 8.3cm)

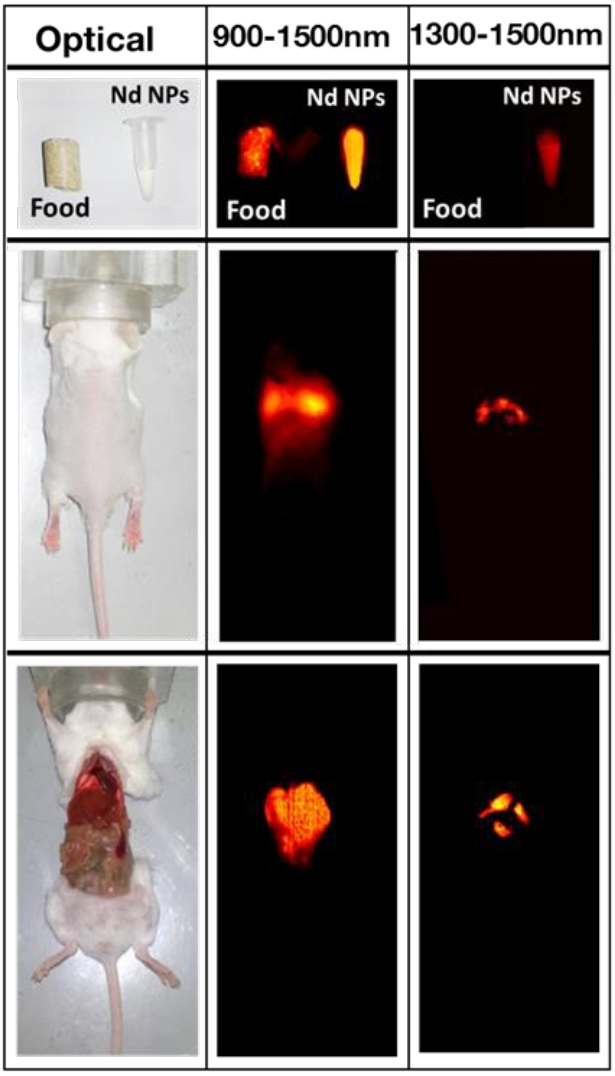

Figure 3. Left column: Optical image of a mouse food pellet, of an Eppendorf containing a colloidal solution of Nd^{3+}:SrF_2 nanoparticles, of a living mouse after intravenous administration through the retro-orbital venous sinus of 50 µL of a colloidal solution of Nd^{3+}:SrF_2 in phosphate buffered saline (PBS), and of the same mouse after being sacrificed and opened to get direct access to organs. Middle column: Corresponding fluorescence images of the three systems under 808 nm illumination as obtained by recording fluorescence in the 900-1500 nm range. Right column: Fluorescence images also obtained under 808 nm excitation but in this case recording fluorescence intensity in the 1300-1500 nm range. Reproduced with permission from ref [69] from Springer.

(SINGLE COLUMN, 8.3 cm)

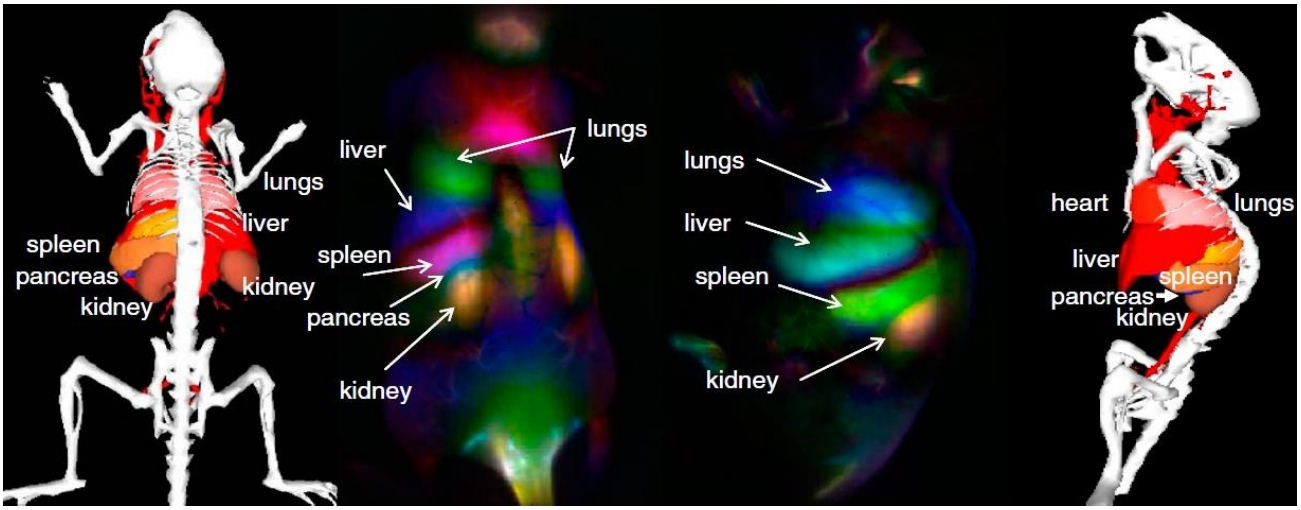

Figure 4. Dynamic contrast-enhanced NIR-II imaging with SWCNTs for increased anatomical resolution of a mouse body. The time-resolved and high-resolution approach allows for the extraction of individual organ information from a seemingly nonspecific signal during imaging. From reference [88] with permission of National Academy of Sciences of US.

(DOUBLE COLUMN, 17.1 cm)

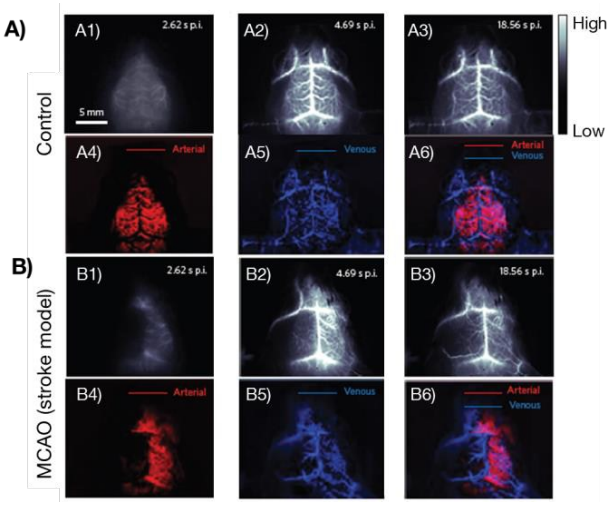

Figure 5. First reported non-invasive and time-resolved SWCNT-based NIR-II imaging (1300-1400 nm wavelength range) of cerebral vasculatures with a spatial resolution of sub-10 µm at a depth of > 2 mm through the skull of mouse. (A) Healthy mouse, (B) mouse with surgically induced middle cerebral artery occlusion (MCAO). Application of the PCA method allows for the distinction between arterial (red) and venous (blue) blood vessels (A3-A6, B3-B6).[92] Reprinted by permission from Macmillan Publishers Ltd: *Nature Photonics*, 8, 723-730. Copyright (2014).

(SINGLE COLUMN, 8.3 cm)

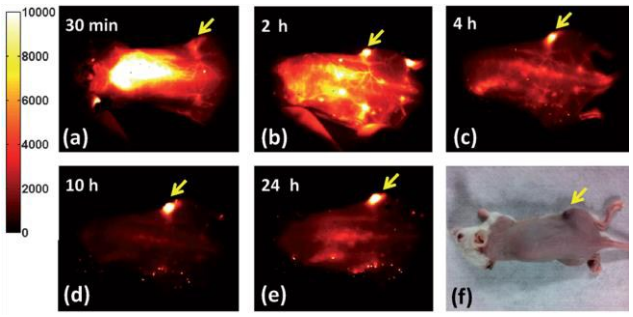

Figure 6. Selective NIR-II imaging reflecting the distribution of PEG-modified Ag_2S QDs inside a xenograft 4T1 tumour bearing mouse, over a longer period of time up to 24 h post tail-vein injection (a-e). Because of the enhanced permeability and retention (EPR) effect of the tumour vasculature, a steady increase of the NIR-II fluorescence from the QDs in the tumour region and a decrease of NIR-II fluorescence in other organs and skin is observed from 30 min to 24 h post-injection, leading to an increased tumour-to-background ratio over time. Reproduced from reference [120] with permission from John Wiley and Sons.

(SINGLE COLUMN, 8.3 cm)

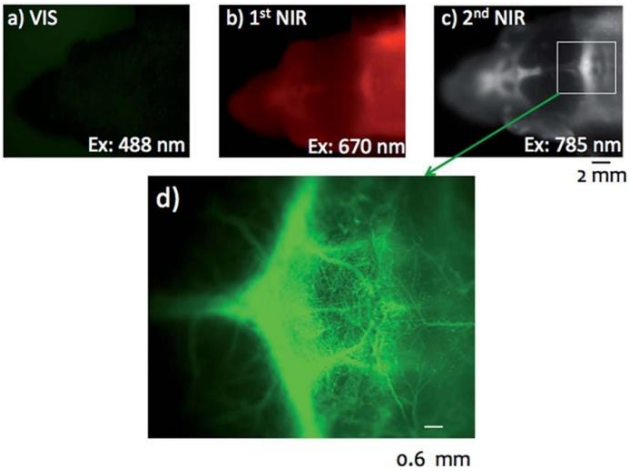

Figure 7. Application of bovine serum albumin (BSA) conjugated VIS, NIR-I and NIR-II PbS/CdS QDs in fluorescence angiography of a mouse head revealing the importance of an appropriate excitation and emission wavelength choice. In comparison to VIS (A) and NIR-I (B), the use of NIR-II (C, D) allows for higher penetration, lower autofluorescence, improved spatial resolution, and increased signal to background ratio, overall resulting in a clearer image of the blood vessels. Reproduced from reference [23] with permission from The Royal Society of Chemistry.

(SINGLE COLUMN, 8.3 cm)

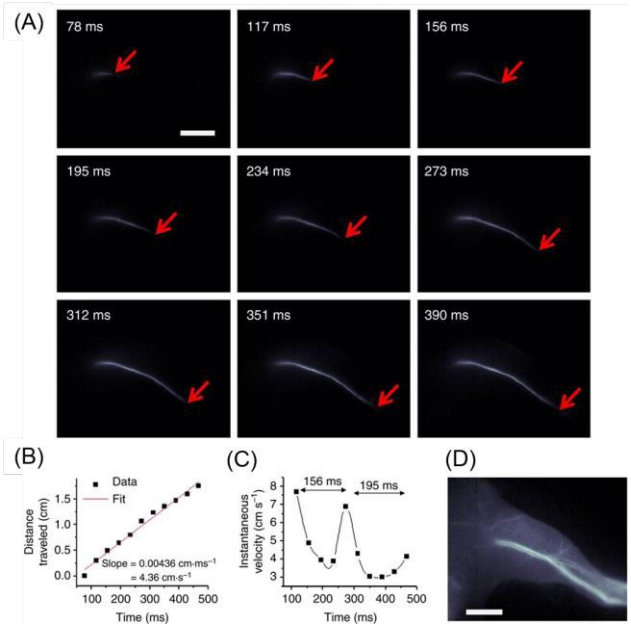

Figure 8. Ultrafast NIR-II imaging of arterial blood flow using PEG-modified copolymer poly(benzo[1,2-b:3,4-b′]difuran-alt-fluorothieno-[3,4-b]thiophene) (named pDA-PEG). (A) A time course of NIR-II fluorescence images of a mouse hindlimb immediately following intravenous injection of pDA-PEG, showing the blood flow front moving inside the femoral artery (indicated by red arrows). The frame rate of imaging is 25.6 f.p.s. with an exposure time of 20 ms and an instrument overhead time of 19 ms. (B) A plot of the distance travelled by the blood flow front as a function of time. The linear fit reveals an average blood velocity of 4.36 cm s^{-1} in the femoral artery. (C) A plot of instantaneous velocity (derived by dividing flow front travelled distance between two consecutive frames by the time interval of 39 ms) as a function of time, revealing periodic changes of instantaneous velocity corresponding to cardiac cycles. (D) An NIR-II fluorescence image of the same mouse hindlimb after full perfusion of pDA-PEG-containing blood into the hindlimb, upon which the fluorescence intensity in the hindlimb became unchanging. The scale bars in (A) and (D) indicate 5 mm.[142] Reprinted by permission from Macmillan Publishers Ltd: *Nature Communications*, 5: 4206. Copyright (2014).

(SINGLE COLUMN, 8.3 cm)

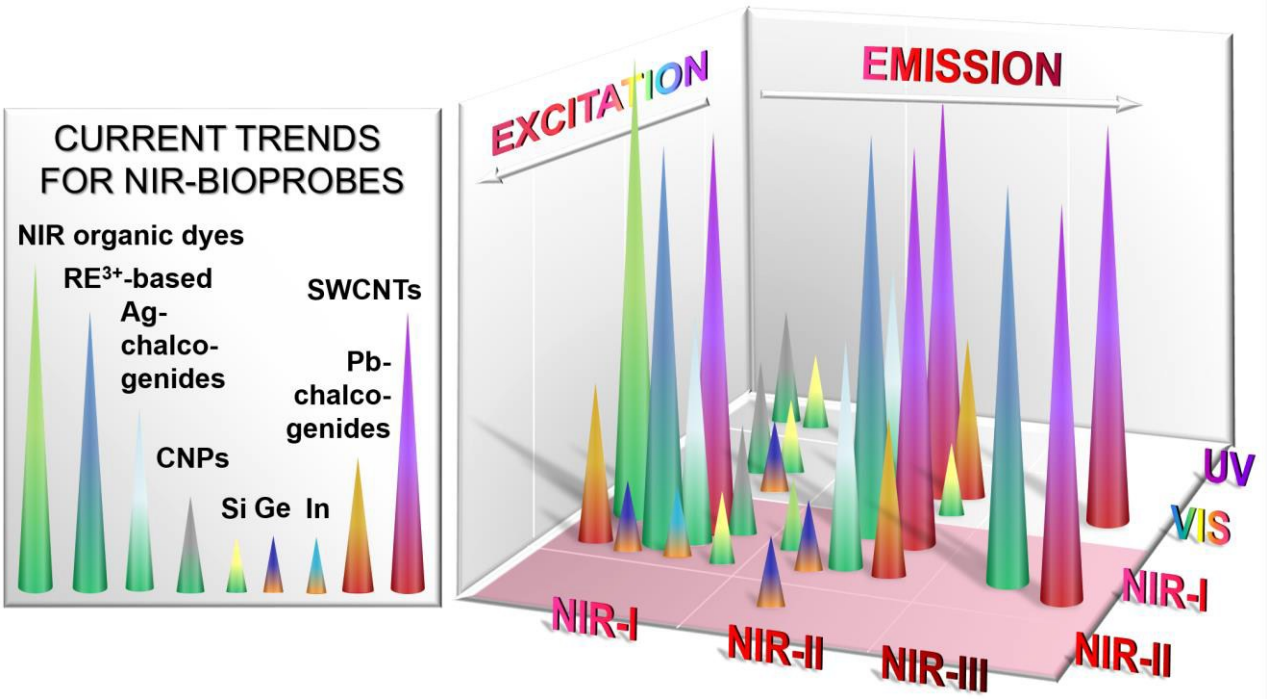

Scheme 2. Achievements and challenges of potential NIR-to-NIR bioprobes for deep-tissue optical imaging. Biocompatibility of the various material classes: A green base indicates reported biocompatibility; an orange base indicates reported concerns; a red base indicates observed *in-vitro*/*in-vivo* toxic effects. The cone height qualitatively represents the stage of development (higher cones indicate higher number in NIR-based *in-vitro*/*in-vivo* studies). The red marked wavelength region represents the NIR *biological windows*.

(DOUBLE COLUMN, 17.1 cm)

FIGURE FOR GRAPHICAL ABSTRACT: 8 cm x 4 cm

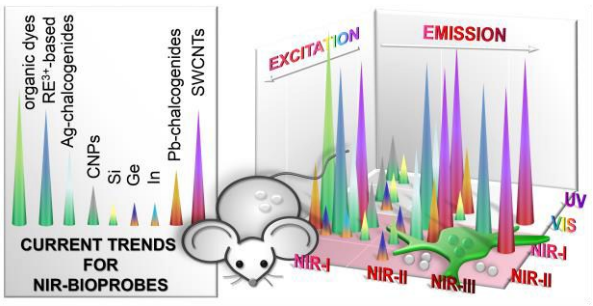

Rare-earth based nanoparticles, Group-IV nanostructures, and novel quantum dots in the near-infrared (NIR) spot-light: Current trends, material merits, and latest developments in NIR-to-NIR bioimaging